



# Pharmacological Inhibition of Brain EGFR Activation By a BBB-penetrating Inhibitor, AZD3759, Attenuates $\alpha$ -synuclein Pathology in a Mouse Model of $\alpha$ -Synuclein Propagation

Omid Tavassoly<sup>1,2</sup> · Esther del Cid Pellitero<sup>2</sup> · Frederique Larroquette<sup>2</sup> · Eddie Cai<sup>2,3</sup> · Rhalena A. Thomas<sup>2,3</sup> · Vincent Soubannier<sup>3</sup> · Wen Luo<sup>3</sup> · Thomas M. Durcan<sup>3</sup> · Edward A. Fon<sup>2</sup>

Accepted: 26 January 2021 / Published online: 12 March 2021  
© The American Society for Experimental NeuroTherapeutics, Inc. 2021

## Abstract

Aggregation and deposition of  $\alpha$ -synuclein ( $\alpha$ -syn) in Lewy bodies within dopamine neurons of substantia nigra (SN) is the pathological hallmark of Parkinson's disease (PD). These toxic  $\alpha$ -syn aggregates are believed to propagate from neuron-to-neuron and spread the  $\alpha$ -syn pathology throughout the brain beyond dopamine neurons in a prion-like manner. Targeting propagation of such  $\alpha$ -syn aggregates is of high interest but requires identifying pathways involving in this process. Evidence from previous Alzheimer's disease reports suggests that EGFR may be involved in the prion-like propagation and seeding of amyloid- $\beta$ . We show here that EGFR regulates the uptake of exogenous  $\alpha$ -syn-PFFs and the levels of endogenous  $\alpha$ -syn in cell cultures and a mouse model of  $\alpha$ -syn propagation, respectively. Thus, we tested the therapeutic potentials of AZD3759, a highly selective BBB-penetrating EGFR inhibitor, in a preclinical mouse model of  $\alpha$ -syn propagation. AZD3759 decreases activated EGFR levels in the brain and reduces phosphorylated  $\alpha$ -synuclein (pSyn) pathology in brain sections, including striatum and SN. As AZD3759 is already in the clinic, this paper's results suggest a possible repositioning of AZD3759 as a disease-modifying approach for PD.

**Keywords**  $\alpha$ -Synuclein · Parkinson's disease · Pre-formed fibrils · Propagation · EGFR-tyrosine-kinase inhibitor · AZD3759

## Introduction

Aggregation and deposition of abnormal proteins in the form of amyloid structures within the brain are among the hallmarks of neurodegenerative diseases. Alzheimer's disease

(AD) and Parkinson's disease (PD) are examples of these disorders in which aggregates of amyloid- $\beta$  ( $A\beta$ ), tau, and  $\alpha$ -synuclein ( $\alpha$ -syn) are deposited within the brain [1–4]. These toxic fibrils have been characterized to act as pathogens and hijack cellular endocytosis pathways to enter cells (uptake). Inside the cells, they serve as a seed to promote aggregation of the endogenous monomeric form of these proteins (seeding). This uptake and seeding process continues from cell-to-cell to transfer amyloid pathology throughout the brain in a prion-like manner (propagation) [4–18]. Targeting the cell-to-cell propagation pathway (a cascade of uptake and seeding) is a therapeutic approach in neurodegenerative diseases to stop or delay pathology development in the brain [4, 19, 20]. In the case of PD, which is the focus of this paper, several receptors and pathways have been identified to involve in the  $\alpha$ -syn-pre-formed-fibrils ( $\alpha$ -syn-PFFs) uptake and propagation [21–24]. However, there are some limitations in therapeutic development targeting these reported mechanisms. For example, some of these pathways such as heparan sulfate proteoglycans (HSPGs) [23] and tunneling

<sup>†</sup>Omid Tavassoly and Esther del Cid Pellitero contributed equally to this work.

✉ Omid Tavassoly  
otavasso@sfu.ca; omid.tavassoly@gmail.com

✉ Edward A. Fon  
ted.fon@mcgill.ca

- 1 Department of Chemistry, Simon Fraser University, Burnaby, BC, Canada
- 2 McGill Parkinson Program and Neurodegenerative Diseases Group, Montreal Neurological Institute, McGill University, Montréal, QC, Canada
- 3 Early Drug Discovery Unit, Montreal Neurological Institute, McGill University, Montréal, QC, Canada

nanotubes [21, 22] might be difficult to target therapeutically, and others only partially mediate the  $\alpha$ -syn uptake and propagation, such as lymphocyte-activation gene-3 (Lag-3) [24]. The latter suggests redundancy, and other unknown mechanisms also mediate the uptake of  $\alpha$ -syn-PFFs. Thus, identifying new pathway(s) that control uptake and propagation of  $\alpha$ -syn-PFFs is of high interest for developing future disease-modifying therapeutics in PD.

A novel target candidate that has predominantly been studied in AD pathology is EGFR [25–29]. Interestingly, there are polymorphisms in the EGFR gene that are associated with the risk of both AD and PD [25, 30]. To emphasize the importance of the role of EGFR in neurodegeneration, we have recently reviewed the potentials of targeting EGFR in the treatment of neurodegenerative diseases [31]. Briefly, EGFR is a tyrosine kinase receptor involved in cellular differentiation and proliferation. The inactive receptor exists as a transmembrane monomer and upon binding to its extracellular ligands, such as epidermal growth factor (EGF) or heparin-binding-EGF-like growth factor (HB-EGF), homodimerizes and undergoes autophosphorylation in its intracellular domain and subsequently internalizes into early endosomes. Activated EGFR triggers the activation of downstream pathways by induction of sequential phosphorylation cascades [31–35]. While mutations and amplification of EGFR are mainly associated with the uncontrolled proliferation of cancer cells, it is also involved in the pathology of diseases such as pathogen infection and neurodegenerative diseases [26, 27, 29, 31–37]. Some viral pathogens exploit the EGFR-mediated endocytosis to enter and infect cells [32–35, 38], and it has been shown that targeting EGFR activation by its specific tyrosine kinase inhibitors reduces viral cellular entry and infectivity [34, 35]. It has also been reported that mutant huntingtin (polyQ-htt) aggregates [39], premelanosome protein (PMEL) fibrils [40], and A $\beta$ -PFFs [37] also bind to EGFR in cell cultures. The binding of ligands to EGFR results in activation of receptor tyrosine kinase activity and its autophosphorylation, which subsequently triggers endocytosis of receptor and ligand. Therefore, direct or indirect hijacking of EGFR-mediated endocytosis is a plausible mechanism of viral or amyloid pathogen entry into cells, suggesting targeting EGFR activation (phosphorylation) using available EGFR-tyrosine kinase inhibitors (EGFR-TKIs) could serve as a novel therapeutic strategy to control endocytosis of pathogens and amyloids [31–35, 38]. However, cancer therapy with these drugs is associated with resistance to the therapy due to autophagy activation [31, 41–45]. In the absence of EGFR-TKIs, EGFR inhibits autophagy [31, 46]. Thus, induction of autophagy by EGFR-TKIs is an adverse effect in cancer therapy, which promotes cancer cells survival [31, 41–45, 47–49], whereas in neurodegenerative diseases, it is beneficial to promote degradation and clearance of abnormal proteins such as

amyloid structures [26, 31]. In fact, this feature of EGFR-TKI therapy has been used to improve A $\beta$  pathologies and memory loss associated with A $\beta$  overexpression in both mice and fly models of AD [26, 27, 29, 37].

Here, we evaluated the beneficial effect of AZD3759, an EGFR-TKI with high BBB penetration [31, 50–54] in PD. We conducted a proof-of-concept study using a propagation mouse model of  $\alpha$ -syn to explore the AZD3759 effect in targeting  $\alpha$ -syn seeding and propagation. We showed that AZD3759 reduces  $\alpha$ -syn-PFFs uptake in vitro and phosphorylated  $\alpha$ -synuclein (pSyn) pathology in vivo. Furthermore, like other EGFR-TKIs [41–46], AZD3759 also activates autophagy in the brain of mice in this study, suggesting a possible mode of action that, together with the reduction in  $\alpha$ -syn-PFFs uptake, ameliorate seeding and propagation of pSyn pathology in the brain. This study brings the opportunity to use AZD3759, which is currently in phase I clinical trials for cancer [31, 50–55], as a new therapy for PD.

## Methods

### Materials

Recombinant human wild-type  $\alpha$ -syn was purchased from AlexoTech (Umea, Sweden). Recombinant mouse wild-type  $\alpha$ -syn was generated using a GST-tagged plasmid. AZD3759 was synthesized, as described previously [53]. Alexa Fluor 647 NHS Ester, Cell Dissociation Buffer (enzyme-free), Pierce™ IP lysis buffer, Hoechst 33342, cell culture media (EMEM, Opti-MEM™, and Neurobasal™ Plus Medium), B-27™ Plus Supplement, and GlutaMAX™ Supplement were purchased from Thermo Fisher Scientific. Methylcellulose (viscosity 4000 cP), phosphatase inhibitor cocktail 2, phosphatase inhibitor cocktail 3, protease inhibitor cocktail, recombinant epidermal growth factor (EGF), anti-p62/SQSTM1 antibody, gefitinib, and HB-EGF were purchased from Sigma (Sigma-Aldrich, St. Louis, MO, USA). CellTiter-Blue® Cell Viability Assay was purchased from Promega Corporation, Madison, WI, USA). EGFR siRNA oligo duplex and universal scrambled negative control (nontarget, NT) siRNA oligo duplex, as well as siRNA transfection reagent (siTran), were purchased from OriGene (OriGene Technologies, Rockville, MD, USA). PathScan® Phospho-EGF Receptor Sandwich ELISA Kit was purchased from Cell Signaling Technology, Inc. (Danvers, MA, USA). Corning™ BioCoat™ Poly-D-Lysine 48-well Plates and Corning® 96-well Half Area High Content Imaging Film Bottom Microplate (#4680) were purchased from Corning Incorporated (Corning, NY, USA). Human neuroblastoma (SK-N-SH) cells were purchased from ATCC (American Type Culture Collection,

Manassas, VA, USA). Primary mouse cortical neurons were purchased from Thermo Fisher Scientific. Purified mouse anti- $\alpha$ -synuclein antibody (clone 42/ $\alpha$ -synuclein) was purchased from BD Biosciences (San Jose, CA, USA). EGFR antibody (A-10), p-EGFR antibody (11C2), and anti-actin antibody (C-2) were purchased from Santa Cruz Biotechnology, Inc. (Dallas, TX, USA). Microtubule-associated proteins 1A/1B light chain 3B (LC3B) antibody was purchased from Novus Biologicals (Littleton, CO, USA). PrimePCR™ SYBR® Green Assay, Sncs, Mouse was purchased from BioRad (Hercules, California, Catalog No. 10025636).

### Fibrillation and Labeling of $\alpha$ -syn

For cell culture studies, human  $\alpha$ -syn-PFFs were generated and labeled with amino-reactive Alexa Fluor 647 NHS Ester as described previously by Tavassoly et al. [56, 57]. Aliquots (500  $\mu$ l of 5 mg/ml in PBS) of recombinant  $\alpha$ -syn monomers were shaken at 1000 rpm in a ThermoMixer at 37°C for 10 days. The generated fibrils were sonicated for 30 s at 10% power (0.5 s on, 0.5 s off). The resulted oligomers ( $\alpha$ -syn-PFFs) were labeled with amino-reactive Alexa Fluor 647 NHS Ester as follows. Alexa Fluor 647 dye was dissolved in DMSO (10 mg/ml), and 100  $\mu$ l of the resulting solution was added to the generated  $\alpha$ -syn-PFFs samples (500  $\mu$ l of 5 mg/ml concentration). Afterward, 60  $\mu$ l (10%, %V/V) of freshly prepared 1 M sodium bicarbonate buffer (pH 8.3) was added to the sample (final volume of 660  $\mu$ l) followed by 2 h incubation at room temperature. Then, the labeled- $\alpha$ -syn-PFFs were purified by dialysis in excess PBS buffer for 12 h.

For animal studies, mouse  $\alpha$ -syn-PFFs were generated based on the Volpicelli-Daley et al. protocol [7]. Recombinant  $\alpha$ -syn-monomers (5 mg/ml in PBS) were incubated in a ThermoMixer (1000 rpm, 37°C) for 5 days, and fibrils were sonicated at high power (10 cycles, 30 s or 60 s) in 10°C water circulation.  $\alpha$ -Syn-PFFs were stored at  $-80^{\circ}\text{C}$  and kept at room temperature during the intracerebral injections.

### Quantitative Reverse-transcriptase PCR

Frozen brain samples were used for this experiment. First brains were homogenized, and RNA was extracted using TRIzol Reagent. Concentrations of extracted RNA were measured using a NanoDrop™ One Microvolume UV–Vis Spectrophotometer (Thermo Scientific™, Waltham, MA), and concentrations were adjusted to 50 ng/ $\mu$ l. Then, 500 ng RNA was used to synthesize cDNA using High Capacity Reverse Transcription Kit (Life Technologies). Afterward, 2  $\mu$ l cDNA was used to perform Real-time PCR with SYBR Green FastMix (Quanta Biosciences, Gaithersburg, MD)

in a QuantStudio™ 3 Real-Time PCR System (Life Technologies, Carlsbad, CA). Gene expression was normalized by total RNA input and expressed as a relative quantity. PrimePCR™ SYBR® Green Assay, Sncs, Mouse (BioRad, Catalog #: 10025636) was used as primers for the PCR reactions.

### Electron Microscopy

Mouse  $\alpha$ -syn-PFFs were characterized using a negative staining protocol and analyzed using an electron microscope. Mouse  $\alpha$ -syn-PFFs were pipetted on a 200 mesh copper carbon grid (3520C-FA, SPI Supplies) and fixed with 4% PFA for 1 min, followed by staining with 2% acetate uranyl (22400-2, EMS) for 1 min. Mouse  $\alpha$ -syn-PFFs were visualized using a transmission electron microscope (FEI Tecnai 12 Bio Twin 120 kV TEM or Tecnai G2 Spirit Twin 120 kV TEM) coupled to a camera (AMT XR80C CCD Camera or Gatan Ultrascan 4000 4 k  $\times$  4 k CCD Camera model 895, respectively). The  $\alpha$ -syn-PFFs length was measured using ImageJ1.5 software, and their distribution was plotted using MATLAB 2017b software.

### Power Analysis

Previous studies demonstrated that 8-week chronic treatment ( $n = 8/\text{group}$ ) of subcutaneous xenograft, leptomeningeal metastasis (LM), and brain metastasis (BM) lung cancer mice models with AZD3759 by oral gavage at a dose of 15 mg/kg/day resulted in significantly superior antitumor activity (100% of animals remained tumor-free) versus mice receiving vehicle with a standard deviation of  $\sim 5\%$  as measured using two-way ANOVA ( $P < 0.0001$ ) [52]. Moreover, a single dose of AZD3759 at 15 mg/kg caused an 89% reduction in p-EGFR levels in leptomeningeal tumor cells 1 h post-treatment in all tested mice ( $n = 5$  mice) [52]. Further, it has been previously demonstrated that control and double transgenic mice with the expression of two mutated AD-linked transgenes (amyloid precursor protein (APP)/presenilin-1(PS1)) ( $n = 4$  per group) manifest a  $\sim 90\%$  reduction in p-EGFR in the brain after 18-day treatment with a less CNS-penetrant EGFR inhibitor (gefitinib) ( $P = 0.05$ ) using a Student *t*-test [37]. It also has been shown that intrastriatal PFFs inoculation of wild-type mice ( $n = 5$ ) at 2 months of age resulted in an increase in pSyn-immunoreactive inclusions with an effect size of 25% versus PBS-injected control mice with a standard deviation of  $\sim 5\%$  as measured using a paired *t*-test ( $P < 0.001$ ). This increase is detectable as early as 30 days post-injection (dpi) [13]. Furthermore, intrastriatal mouse- $\alpha$ -syn-PFFs-inoculation of wild-type mice ( $n = 5$ ) at 2 months of age causes an increase in the proportion of substantia nigra (SN) dopaminergic neurons (DA)

containing pSyn-positive inclusions with an effect size of 28% versus human- $\alpha$ -syn-PFFs-injected mice with a standard deviation of ~5% as measured using two-way ANOVA (Tukey's HSD method) ( $P < 0.001$ ) [5]. This increase was detected at 30 dpi and increased over time ( $\alpha$ -syn-PFFs-induced inclusions peak in the SN at 2 months following intra-striatal injection) [5, 13, 58, 59]. Guided by previous studies (see above) using  $\alpha$ -syn-PFFs-inoculated wild-type mice [13, 58, 59], AD mice models [26, 27, 37], and reports using AZD3759 [52, 53], we found using G\*Power software [60, 61] that at least 6 mice are needed in each group ( $P = 0.05$ , power = 80%) to detect a minimum statistically significant difference of at least 30% (SD = 5%) between the 6 study groups. This allowed a 10% dropout rate and assumed using one-way ANOVA in the following endpoints; (a) decrease in p-EGFR level and (b) reduction in the level of pSyn. Therefore, our study was well powered to observe a range of treatment effects and test the proposed hypotheses.

### Stereotaxic Injection

Male C57/B6C3F1 mice (15–20 g, 4 weeks old; Jackson laboratory, [B6C3F1/J, Stock No. 100010]) were housed and maintained on a 12/12 h light/dark cycle at 22°C ambient temperature and with unlimited access to food and water. Housing and procedures were performed according to the Canadian Council on Animal Care and were approved by the McGill University Animal Care Committee.

Stereotaxic injection of PBS or  $\alpha$ -syn-PFFs performed at 7 or 8 weeks of age. Mice were anesthetized with 2% isoflurane, and a dose of 20 mg/kg carprofen and 250 mg/ml bupivacaine were administered subcutaneously before the craniotomy. Mouse  $\alpha$ -syn-PFFs (total protein concentration of 12.5  $\mu$ g per brain) [62–64] or phosphate-buffered saline (PBS) were microinjected unilaterally (0.25  $\mu$ l during 10 min using a 5  $\mu$ l Hamilton syringe with a 33 gauge needle) in the right dorsal striatum (+0.2 mm relative to bregma, +2.0 mm lateral from midline, and 2.6 mm ventral from dorsal skull surface using the bregma as a reference point) based on previously described methods [12].

### Chronic Pharmacodynamic Study

We expected that sustained inhibition of EGFR is needed to block PD progression in this mouse model. To test this idea, we used male wild-type mice (C57BL6/C3H) ( $n = 20$ ) inoculated with  $\alpha$ -syn-PFFs ( $n = 10$ ) or PBS ( $n = 10$ ) by injection into the striatum (see above) and dosed half ( $n = 5$ ) of each group with AZD3759 (15 mg/kg/day) over 21 days. Briefly, mice at 6 weeks of age received placebo (1% methylcellulose,  $n = 10$ ) or AZD3759 (15 mg/kg/day,  $n = 10$ ) using a gavage needle (FNS-20-1.5.2, Kent Scientific Corporation)

for 7 days. Then, at 7 weeks of age, they received an intracerebral (i.c.) injection of PBS or mouse- $\alpha$ -syn-PFFs (Fig. S1e, f,  $n = 10$ ). After 5 days of recovering, AZD3759, or placebo, was re-administrated to mice for an additional 14 days (Fig. 3a). Afterward, mice were anesthetized with 5% isoflurane, followed by 7% CO<sub>2</sub>. Then, brains were removed from the cranium and quickly froze in liquid nitrogen (flash-freezing). Brains were stored at  $-80^{\circ}\text{C}$  until they were analyzed by immunoblotting and quantitative reverse-transcriptase PCR.

### Proof-of-concept Study

The study was blinded to drug treatment. For this study, we used 49 male wild-type mice (C57BL6/C3H F1). In this model, a single unilateral injection of PFFs into the striatum induces neurochemical and pathological features of synucleinopathy within 1–6 months [13, 58, 59]. In terms of pathology, pSyn-positive Lewy body (LB)-like inclusions are detected as early as 30 dpi at the site of injection in the striatum and spread to other areas such as the neocortex and olfactory mitral neurons ipsilateral to the injection site. Furthermore, pSyn pathology in substantia nigra (SN) developed as pale cytoplasmic accumulations as early as 30 dpi [13, 58, 59]. Thus, this model fitted well with our planned dosing period (~60 dpi), adopted from mice cancer therapy using AZD3759 [52]. Therefore, any therapeutic effect of AZD3759 to reduce  $\alpha$ -syn seeding and propagation (pSyn pathology) should be detectable in our study. Mice at 6 weeks of age were administrated with placebo ( $n = 16$ ) or AZD 3759 [0.64 mg/kg/day ( $n = 16$ ) or 8.6 mg/kg/day ( $n = 17$ )] using a gavage needle for 15 days. At 8 weeks of age, they received an i.c. injection of PBS or mouse- $\alpha$ -syn-PFFs (60 s sonication,  $n = 7$ –9 per group) (Fig. S1g, h). After 10 days of recovering, mice were re-administrated with placebo or AZD3759 (0.64 mg/kg/day or 8.6 mg/kg/day) for an additional 60 days (Fig. 4a). Then, mice were anesthetized with 2% isoflurane and were perfused intracardially with 10% formalin. The brains were removed and post-fixed with 10% formalin for 24 h at 4°C. Coronal sections containing the striatum and substantia nigra were cut with a paraffin microtome at 5  $\mu$ m thickness and processed for immunohistochemistry and immunofluorescent.

### Immunohistochemistry

For pSyn immunohistochemistry, tissue sections were incubated in citrate buffer (pH: 6.0) for 10 min, rinsed with Tris buffered saline containing 0.1% Tween-20 (TBST), and incubated in 3% oxidase peroxidase for 15 min. Subsequently, the sections were blocked with 10% normal goat serum in TBST for 30 min at room temperature and incubated with anti-phospho-S129- $\alpha$ -synuclein antibody (Abcam: P-syn/81A-ab184674, 1:500) overnight at 4°C. Afterward, the sections

were incubated in secondary antibody, goat anti-mouse-HRP (1:500) for 30 min. The peroxidase reaction product was visualized as a brown precipitate by incubating the tissue with the DAB substrate kit (8059, Cell Signal Technology).

Sections were incubated in hematoxylin to stain the nuclei of the cells. Immunohistochemistry of sections was examined by a bright-field microscope (Olympus DP-21SAL coupled to a digital camera DP21/DP26).

### Immunofluorescence of Brain Sections

Tissue sections were incubated in citrate buffer (pH: 6.0) for 10 min, rinsed with TBST, and incubated in 3% oxidase peroxidase for 15 min. The sections were blocked with 10% normal donkey serum in TBST for 30 min at room temperature and incubated with anti-phosphorylated pS129  $\alpha$ -synuclein antibody (Abcam: ab184674, 1:500) and anti-tyrosine hydroxylase antibody (Millipore: ab152, 1:500) overnight at 4°C. The sections were incubated in secondary antibody, donkey anti-mouse 488 nm (Thermo Fisher: A21202, 1:500), and goat anti-rabbit 555 nm (Thermo Fisher: A-21429, 1:500) for 2 h at room temperature. Coronal sections were examined using a Zeiss Axio Observer Z1 microscope.

### AZD3759 Formulation

AZD3759 was formulated as a suspension in 1% methylcellulose based on mice average weight, administrated dose (placebo or 0.64 mg/kg/day or 8.6 mg/kg/day), and volume of oral gavage per day per mouse (250  $\mu$ l). Some methylcellulose powder (20 g) was first autoclaved for this formulation. For 100 ml of suspension, formulation performed as follows. The required amount (mg) of AZD3759 was transferred in a conical centrifuge tube (50 ml). Then, 45 ml of water was added to the tube containing AZD3759, followed by sonication at 50% power for 1 min (30 s on/30 s off). Then, the tube was kept in the fridge for at least 2 h. Next, 45 ml of boiled water was poured in a clean and autoclaved Erlenmeyer flask (125 ml) containing a magnetic spinner bar. Autoclaved methylcellulose (1 g) was added to the flask agitated by the magnetic spinner bar. Agitation continued until the temperature reached 56°C. Then, the cold AZD3759 mixture was added to the flask. Agitation continued for 20 min, and then, the final volume was adjusted to 100 ml by adding cold water. Afterward, the suspension was sonicated at 50% power for 1 min (30 s on/30 s off). To remove bubbles, the suspension was kept at -20°C for 2 min.

### Cellular Uptake Assays

Cellular uptake assay for Alexa Fluor 647-labeled- $\alpha$ -syn-PFFs was performed as described previously [56]. SK-N-SH cells were maintained in EMEM, supplemented with 10%

FBS (Gibco, Thermo Fisher Scientific) and 100  $\mu$ g/ml penicillin/streptomycin. Cells were seeded at  $5 \times 10^3$  cells per well in a 96-well plate (Corning 4680, Corning, NY, USA) and were incubated at 37°C with 5% CO<sub>2</sub> overnight. Cells were starved for 2 h and then were treated with different concentrations of HB-EGF or EGF (0.3125  $\mu$ g/ml, 0.625  $\mu$ g/ml, 1.25  $\mu$ g/ml, 2.5  $\mu$ g/ml, 5  $\mu$ g/ml, 10  $\mu$ g/ml, 20  $\mu$ g/ml) for 20 min. Next, the media was aspirated and replaced with fresh media to remove unbound and excess ligands before Alexa Fluor 647-labeled- $\alpha$ -syn-PFFs treatment. Afterward, Alexa Fluor 647-labeled- $\alpha$ -syn-PFFs (100 nM corresponding to monomer concentration before fibrillation) were added as required to a subset of wells. Then, after 6 h incubation with  $\alpha$ -syn-PFFs, cells were washed with trypsin (0.01% trypsin in media) [56] followed by washing with PBS (three times) to remove extracellular and excess fluorescent-labeled- $\alpha$ -syn-PFFs. Finally, cells were fixed with 4% paraformaldehyde (PFA) for quantitative uptake assays using high-content fluorescence microscopy. Additionally, 1 h before fixation, Hoechst 33342 (1: 50,000 ratio; Thermo Fisher Scientific, H3570) was added to each well to stain nuclear.

### Neuronal Culture and $\alpha$ -syn-PFFs Uptake Assay

This assay was performed as described previously by Tavassoly et al. [56]. Primary mouse cortical neurons were maintained in complete Neurobasal™ Plus Medium supplemented with B-27™ Plus Supplement (20 mL/L) and GlutaMAX™ Supplement (2.5 mL/L). Cells were plated at  $5 \times 10^3$  cells per well in a 96-well plate (Corning 4680) coated with poly-L-lysine and incubated at 37°C with 5% CO<sub>2</sub>. Twenty-four hours after initial incubation, half of the medium from each well were removed and replaced with freshly prepared complete medium. This media replacement was repeated every third day for 21 days. At this time, neurons were treated with AZD3759 (0.63 nM or 8.4 nM) or gefitinib (8.4 nM) or vehicle alone. After 4 h incubation with EGFR inhibitor, neurons were then treated with Alexa Fluor 647-labeled- $\alpha$ -syn-PFFs (100 nM) and were then incubated at 37°C for 6 h. Hoechst 33342 (1: 50,000 ratio; Thermo Fisher Scientific, H3570) was added to each well 1 h before washing/fixing the cells. After washing, cells were fixed with 4% PFA to perform quantitative uptake assays using high-content fluorescence microscopy.

### Neuronal Inhibition of EGFR Phosphorylation By AZD3759

This assay was described for cancer cells by Zheng et al. [53]. We adjusted the original protocol to be used for mice primary neurons. Briefly, primary mouse cortical neurons were maintained in complete Neurobasal™ Plus Medium

supplemented with B-27™ Plus Supplement (20 mL/L) and GlutaMAX™ Supplement (2.5 mL/L). Cells were plated at  $0.5 \times 10^5$  live cells per well in a poly-D-lysine-coated 48-well plate and incubated at 37°C with 5% CO<sub>2</sub>. Twenty-four hours after initial incubation, half of the medium from each well was aspirated and replaced with fresh medium. This media replacement was repeated every third day for 21 days. For the ELISA experiments, cells were starved (incubation with Neurobasal™ Plus Medium with no supplement) for 2 h and then exposed to AZD3759 at concentrations ranging from 10 to  $1.19209 \times 10^{-6}$  mM. After 4 h of incubation, cells were stimulated with EGF (100 ng/ml) for 20 min. Then, the media were aspirated, and 110 µL of Pierce IP lysis buffer, including phosphatase inhibitor cocktail 2 and 3 (1:100 ratio dilution of each cocktail) as well as protease inhibitor cocktail (1:100 dilution), were added to each well. After 1 h incubation, an ELISA Kit (Cell Signaling Phospho-EGF Receptor Sandwich ELISA Kit) was used to measure the level of p-EGFR inhibition in the resulted cell lysates using a plate reader by recording the absorbance at 450 nm. IC values (IC<sub>20</sub> and IC<sub>50</sub>) were measured by fitting data in OriginPro 8.0.

### Cell Viability Assay

Cell viability was evaluated with a fluorimetric test using CellTiter-Blue® Cell Viability Assay (Promega), according to the manufacturer's instructions. Briefly, mouse primary neurons were seeded at  $5 \times 10^3$  in black 96-well flat-bottom plates pre-coated with poly-L-Lysine and were maintained for 21 days (see above). AZD3759 was added in a range of 0.47–30 µM. After 3 h and 23 h incubation with AZD3759, CellTiter-Blue® Reagent (20 µl) was added to each well and incubated for an additional 1 h. Fluorescence (560Ex/590Em) was determined using a SPARK® Multimode Microplate Reader (Tecan™).

### Automated Microscopy Analysis

A high-content imaging system (ImageXpress Micro XLS; Molecular Devices, San Jose, CA, USA) was used to image cells automatically as described previously [56, 57]. Imaging involved selection of nonoverlapping fields (12 different fields) per well to be imaged automatically. Analysis of recorded images was performed using the MetaXpress (Molecular Devices). This software quantified the number, area, and intensity of uptaken  $\alpha$ -syn-PFFs in recorded images. Then, to obtain uptake level per cell, intensity signals were normalized to the number of cells. Next, mean intensities for each treatment were normalized to the level of  $\alpha$ -syn-PFFs uptake in cells with no treatment (control). The data points are presented as mean  $\pm$  SD. The results represent three independent biological repeats.

### Quantification of Marker Signals in Mice Sections

Coronal sections of the striatum and substantia nigra processed for immunohistochemistry or immunofluorescence were analyzed using Fiji-ImageJ 1.53 software. Macros for Fiji-ImageJ were written in Jython, using basic ImageJ functions [65], to preprocess batches of coronal sections by masking non-tissue areas, labelling the images and to detect the total area of profiles labeled. For immunohistochemistry, color deconvolution was performed to separate hematoxylin and DAB staining, and the total area of DAB staining was determined as well as the total area of the tissue section. Data are expressed as total staining area/total tissue area. The percentage of pSyn<sup>+</sup> cells was normalized to the average of pSyn<sup>+</sup> cells of the Placebo- $\alpha$ -syn-PFFs group [(number of pSyn<sup>+</sup> cells/average of pSyn<sup>+</sup> cells of the Placebo- $\alpha$ -syn-PFFs group)  $\times$  100]. For immunofluorescence, channels from each image were separated. For each channel, a set threshold was applied and total signal intensity and area were measured. Masks were created and superimposed to obtain percentages of colocalized signal areas between channels. Data are expressed as percentages of colocalized areas. The analysis macro is available on Github <https://github.com/neuroeddu/HistQ>. The percentage of TH<sup>+</sup> cells was normalized to the average of TH<sup>+</sup> cells of the Placebo-PBS group [(number of TH<sup>+</sup> cells/ average of TH<sup>+</sup> cells of the Placebo-PBS group)  $\times$  100].

### Knock-down Experiments

siRNA transfections were performed as described previously [56]. SK-N-SH cells were seeded at  $3.5 \times 10^5$  in tissue culture dishes (100 mm) containing 10 ml of transfection media. Opti-MEM supplemented with 10% FBS and 1% penicillin/streptomycin was used for siRNA transfections. Transfection media was composed of: 12 nM siRNA oligo duplex (EGFR siRNA or NT siRNA) and 0.2% transfection reagent (siTran) in complete Opti-MEM. Cells were incubated at 37°C for 48 h, followed by another transfection. Cells were incubated for additional 48 h after the second transfection. Then, cells were detached using cell dissociation buffer (enzyme-free) and transferred into 96-well plates (Corning 4680) for quantitative uptake assay using high-content fluorescence microscopy (see above) or lysed for immunoblotting.

### Gel Electrophoresis and Immunoblotting

Cell and brain lysates were prepared in a buffer containing 50 mM Tris-HCl (pH, 8), 274 mM NaCl, 5 mM KCl, 2 mM EDTA, 2 mM EGTA, one complete-mini protease inhibitor tablet (Roche) per 50 ml, 5 mM sodium pyrophosphate,

30 mM  $\beta$ -glycerophosphate, 30 mM sodium fluoride, and 1 mM phenylmethylsulfonyl fluoride (PMSF). For immunoblotting, cell lysates (40  $\mu$ g) or whole-brain lysates (25  $\mu$ g) were loaded and electrophoresed on a gradient SDS–polyacrylamide gel (4–15%, BioRad), followed by transferring onto a nitrocellulose membrane (pore size 0.45  $\mu$ m). For  $\alpha$ -syn and pSyn immunoblotting, the membrane was incubated in diluted PFA (0.4% in PBS) for 30 min at room temperature before blocking with milk [66]. The membrane was then blocked for 1 h with 5% skim milk (BioRad) in PBS containing 0.1% Tween-20 (PBS-T) at room temperature followed by overnight incubation with a primary antibody in PBS-T containing 1% skim milk at 4°C. As primary antibody, mouse monoclonal anti- $\alpha$ -synuclein antibody (clone 42/ $\alpha$ -synuclein), anti-phosphorylated- $\alpha$ -synuclein (phospho S129) antibody [EP1536Y] (ab51253, Abcam), anti-EGFR antibody (A-10), anti-p62/SQSTM1 antibody, anti-LC3B antibody, anti-p-EGFR antibody (11C2), and anti-actin antibody (C-2) were used at a dilution of 1:1000. The membrane was then washed (three times, 5 min each) with PBS-T containing 1% skim milk. Afterward, the membrane was incubated with a fluorescent-labeled secondary anti-mouse IgG antibody (at a dilution of 1:20,000) in PBS-T containing 1% skim milk at room temperature for 1 h. After washing with PBS-T (three times, 10 min each), an LI-COR Odyssey® Infrared Imaging System was used to detect immunoreactive protein bands on the membrane.

### CD Spectroscopy and ThT Fluorescence Analysis of Human $\alpha$ -synuclein

Circular dichroism (CD) spectra were recorded as previously described by Tavassoly et al. [56, 57, 67–69]. Dilutions of human  $\alpha$ -syn monomers and fibrils (5  $\mu$ M) were prepared in sodium phosphate buffer (10 mM, pH 7.4). Aliquots of samples were transferred to a cell (0.2-cm path length), and the CD spectra of samples were collected over a range of 190–260 nm on an Applied Photophysics CHIRASCAN PLUS CD Spectrophotometer equipped with a Quantum Northwest TC125 temperature controller at 22°C. A blank measurement of buffer was collected to correct the recorded data. The results are expressed as mean residue ellipticity in deg cm<sup>2</sup> dmol<sup>-1</sup>. For the ThT fluorescence study, aliquots of  $\alpha$ -syn samples were collected at different time points (0 h, 8 h, 24 h, 48 h, 72 h, 96 h, 120 h, 144 h, and 168 h) during the fibrillation process. A reading sample was prepared for each time point containing  $\alpha$ -syn (50  $\mu$ M) and ThT (40  $\mu$ M) in PBS. Final volumes of 150  $\mu$ l of each sample were transferred in a 96-well plate. The excitation wavelength was set to 450 nm, and emission was recorded at 480 nm using a SPARK® Multimode Microplate Reader (Tecan™). Blank measurements of buffer and ThT solution were collected to correct the recorded data [57].

### Atomic Force Microscopy

A Bruker atomic force microscope (Dimension Icon) was used to image the morphology of human  $\alpha$ -syn fibrils before and after fibrillation [56]. Briefly, 150  $\mu$ l of diluted fibrils (50  $\mu$ M in PBS) was added onto the surface of a mica disc (SPI Chem Mica, Grade V-4) and left for 15 min at room temperature. Then, fibril solution was aspirated from the mica, and the mica was rinsed with water. The slow flow of N<sub>2</sub> gas was used to dry the surface of mica. Afterward, the mica surface was scanned using “ScanAsyst in Air” mode by a Standard Tapping Mode AFM Probe (Nanosensors, PPP-NCHR).

### Statistical Analysis

All data are reported as “mean  $\pm$  SD.” The Student’s *t*-test was used for statistical comparisons between control (no treatment in cell cultures or placebo in the animal study) and treated conditions (treated cells or drug administrated mouse group). A one-way ANOVA analysis with Tukey’s HSD post hoc tests was used to determine statistical significance changes within groups and multiple comparisons between study groups. GraphPad Prism 7 was used for all statistical analysis and graphs preparation. *P* < 0.05 was considered statistically significant. \**P*  $\leq$  0.05, \*\**P*  $\leq$  0.01, \*\*\**P*  $\leq$  0.001, and \*\*\*\**P*  $\leq$  0.0001.

## Results

### EGFR Inhibition in Cells Reduces $\alpha$ -syn-PFFs Uptake

To address the role of EGFR in PD pathology, we first studied the role of EGFR in the cellular uptake of  $\alpha$ -syn-PFFs as a possible mechanism for targeting EGFR in PD. Therefore, human  $\alpha$ -syn-PFFs were generated and characterized using atomic force microscopy (AFM), circular dichroism (CD) spectroscopy, and thioflavin T (ThT) assay (Fig. S1). AFM images showed the morphology of intact fibrils (Fig. S1a) as typical long fibril structures. Sonication of these fibrils caused the breaking of intact structures and resulted in the formation of smaller fibrils ( $\alpha$ -syn-PFFs) (Fig. S1b). Furthermore, both CD spectroscopy (Fig. S1c) and ThT assay (Fig. S1d) confirmed the formation of  $\beta$ -sheet structures after fibrillation. Then,  $\alpha$ -syn-PFFs were labeled with Alexa Fluor 647 and were used in all subsequent  $\alpha$ -syn-PFFs uptake assays. We determined  $\alpha$ -syn-PFFs uptake in a human neuroblastoma cell line (SK-N-SH) and primary mouse cortical neurons using an uptake assay characterized in our recently published paper [56]. Briefly, we treated cells with 100 nM of Alexa Fluor 647-labeled  $\alpha$ -syn-PFFs (corresponding to protein concentration before fibrillation)

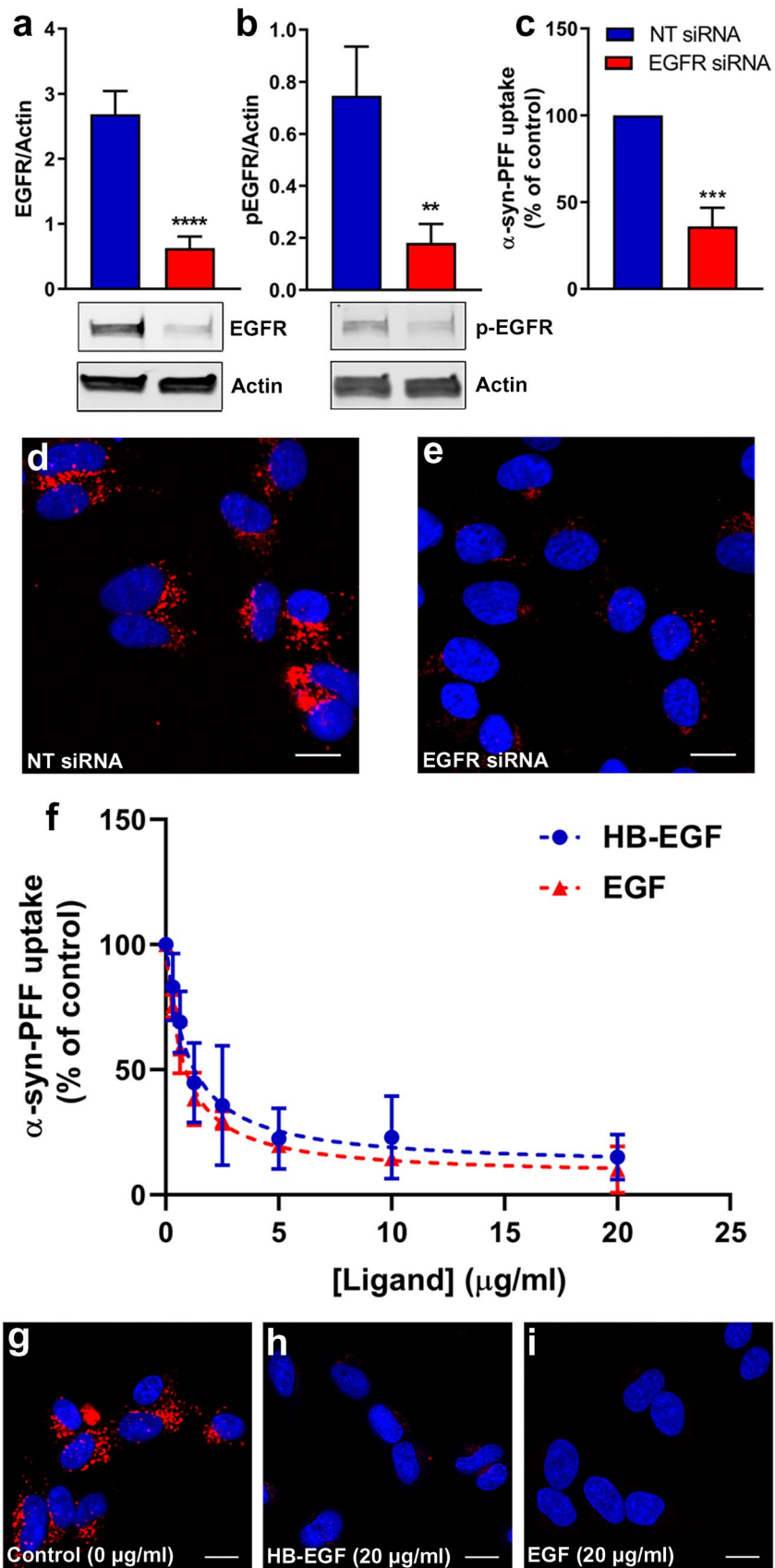




**Fig. 1** Effect of EGFR knockdown and ligand (HB-EGF and EGF) treatment on  $\alpha$ -syn-PFFs uptake. **a** Immunoblot analysis and quantification of EGFR protein levels in SK-N-SH cell lysates after knocking down EGFR using specific siRNA oligo duplex showing the efficacy of knockdown as compared to cells treated with a nontarget (NT) siRNA oligo duplex as control ( $n=3$ ). **b** Immunoblot analyses of p-EGFR levels and quantification after knocking down EGFR using siRNA compared to cells treated with a NT siRNA oligo duplex as control ( $n=3$ ). **c** Quantification of high-content cellular analysis showing the effects of targeted siRNA knockdown of EGFR on uptake of  $\alpha$ -syn-PFFs (100 nM, 6 h incubation) compared to an NT siRNA oligo duplex as control. **d, e** High-content cellular analysis images representing the results shown in **c** ( $n=3$ ). In each single replicate, 12 different automatically preassigned nonoverlapping fields in each well (eight wells for each condition) were imaged. Images from these fields for each condition were selected as representative images. DAPI channel (nucleus) and Cy5 channel ( $\alpha$ -syn-PFFs) are represented in blue and red, respectively. The scale bar represents 10  $\mu$ m (\*\* $P \leq 0.01$ , \*\*\* $P \leq 0.001$ , and \*\*\*\* $P \leq 0.0001$ ). The results in **a–e** represent three independent biological repeats ( $n=3$ ). Error bars represent mean  $\pm$  SD. The Student's *t*-test was used for statistical comparisons between control (NT-siRNA) and EGFR siRNA. **f** SK-N-SH cells were treated with different concentrations of HB-EGF or EGF (0  $\mu$ g/ml, 0.3125  $\mu$ g/ml, 0.625  $\mu$ g/ml, 1.25  $\mu$ g/ml, 2.5  $\mu$ g/ml, 5  $\mu$ g/ml, 10  $\mu$ g/ml, 20  $\mu$ g/ml) for 20 min and then incubated with  $\alpha$ -syn-PFFs (100 nM) for 6 h. The level of  $\alpha$ -syn-PFFs uptake was measured by high-content cellular analysis. IC<sub>50</sub> values of HB-EGF and EGF to antagonize  $\alpha$ -syn-PFFs uptake were measured as 1  $\mu$ g/ml and 0.7  $\mu$ g/ml, respectively. **g–i** Representative high-content cellular analysis images of untreated cells (**g**) and cells treated with HB-EGF (20  $\mu$ g/ml) (**h**) and EGF (20  $\mu$ g/ml) (**i**). DAPI channel (nucleus) and Cy5 channel (Alexa Fluor 647-labeled  $\alpha$ -syn-PFFs) are represented in blue and red, respectively. The scale bar represents 10  $\mu$ m

and measured the fluorescent internalized after 6 h by high-content fluorescence microscopy [56]. To test if EGFR is involved in the uptake of  $\alpha$ -syn-PFFs, we used siRNA to knockdown EGFR in SK-N-SH cells (Fig. 1a–e). Immunoblot analysis of cell lysates showed that knockdown of EGFR reduced both total and phosphorylated EGFR (Fig. 1a, b). We found siRNA-driven knockdown of EGFR resulted in a 64% reduction in the level of  $\alpha$ -syn-PFFs uptake (Fig. 1c–e). To further test if EGFR is involved in  $\alpha$ -syn-PFFs uptake, we incubated starved SK-N-SH cells with different concentrations of high-affinity EGFR ligands, HB-EGF or EGF, for 20 min followed by washing with PBS to remove excess unbound ligands and then treatment with fresh media containing  $\alpha$ -syn-PFFs (100 nM). After 6 h incubation, the level of  $\alpha$ -syn-PFFs uptake was measured by high-content imaging (Fig. 1f–i). These results showed that HB-EGF and EGF antagonize  $\alpha$ -syn-PFFs uptake in a concentration-dependent manner (IC<sub>50</sub> ~ 1  $\mu$ g/ml and 0.7  $\mu$ g/ml, respectively) and suggest that  $\alpha$ -syn-PFFs compete with EGFR ligands to bind to the receptor and activate the receptor. Thus, this activation was evaluated in mice primary neurons by incubation of starved cells with  $\alpha$ -syn-PFFs at two time points (10 min and 30 min) and measuring the level of EGFR activation by immunoblotting (Fig. S4). Results showed EGFR activation over time by  $\alpha$ -syn-PFFs. Next, we

tested if targeting EGFR activation in neurons by AZD3759 also reduces the cellular entry of  $\alpha$ -syn-PFFs in primary mouse cortical neurons. As this inhibitor, AZD3759, was developed for brain cancer therapy, all pharmacokinetics and pharmacodynamics (PK and PD) properties have been characterized in cancer-related cell lines and animal models with mutated EGFR or amplified wild-type EGFR [52, 53]. Thus, we measured IC<sub>20</sub> and IC<sub>50</sub> (drug concentration causing 20% and 50% inhibition of p-EGFR, respectively) and LD<sub>50</sub> (drug concentration causing 50% cell viability) of AZD3759 in mouse primary cortical neurons. We obtained IC<sub>20</sub> and IC<sub>50</sub> values as 0.63 nM and 8.4 nM, respectively, and LD<sub>50</sub> of 5  $\mu$ M and 4.7  $\mu$ M after 4-h and 24 h incubation times, respectively (Fig. 2a, b). These values were similar to the range of reported value for IC<sub>50</sub> in cancer cells but lower than the reported LD<sub>50</sub> values [44, 45], suggesting that AZD3759 may be suitable to attenuate  $\alpha$ -syn-PFFs uptake in neurons and in vivo. Therefore, we treated mouse cortical neurons with AZD3759 (0.63 nM and 8.4 nM) for 4 h, followed by  $\alpha$ -syn-PFFs (100 nM) treatment. After 6 h incubation with  $\alpha$ -syn-PFFs, cells were washed, fixed, and imaged by high-content fluorescence microscopy. Images of neurons at the end of the experiment before fixation showed typical healthy neurons even in the presence of AZD3759 (Fig. 2d–f). Quantification of high-content cellular analysis of  $\alpha$ -syn-PFFs uptake showed a 33% and 48% reduction in the level of  $\alpha$ -syn-PFFs uptake in the presence of 0.63 nM and 8.4 nM of AZD3759, respectively (Fig. 2c, g–i), indicating that inhibition of EGFR activation reduces the uptake of  $\alpha$ -syn-PFFs uptake in neurons. Furthermore, to validate that activation and autophosphorylation of EGFR by its tyrosine kinase activity mediates endocytosis of  $\alpha$ -syn-PFFs, another EGFR-TKI (gefitinib) was used in the same uptake assay (see above) (Fig. S6). Results showed that similar to AZD3759, inhibition of EGFR tyrosine kinase activity and phosphorylation by gefitinib (8.4 nM) resulted in a reduction in the level of  $\alpha$ -syn-PFF uptake comparable to the inhibitory effect of AZD3759 (8.4 nM).

### EGFR inhibition in a mouse model of $\alpha$ -syn propagation ameliorates pSyn pathology

Next, we performed a short-term pharmacodynamics study to test whether AZD3759 reduces EGFR activation in vivo using a well-characterized wild-type mouse  $\alpha$ -syn-propagation model (C57BL/6/C3H F1 mice inoculated with mouse- $\alpha$ -syn-PFFs (average fibril length: 50.71 nm)) [13, 58, 59]. AZD3759 or placebo (1% methylcellulose) was administered by oral gavage to 10 mice (5 wild-type mice injected with PBS and 5 wild-type mice injected with  $\alpha$ -syn-PFFs) at 15 mg/kg/day as indicated in Fig. 3a. Immunoblotting of brain lysates from these animals revealed that AZD3759 reduced the levels of p-EGFR as

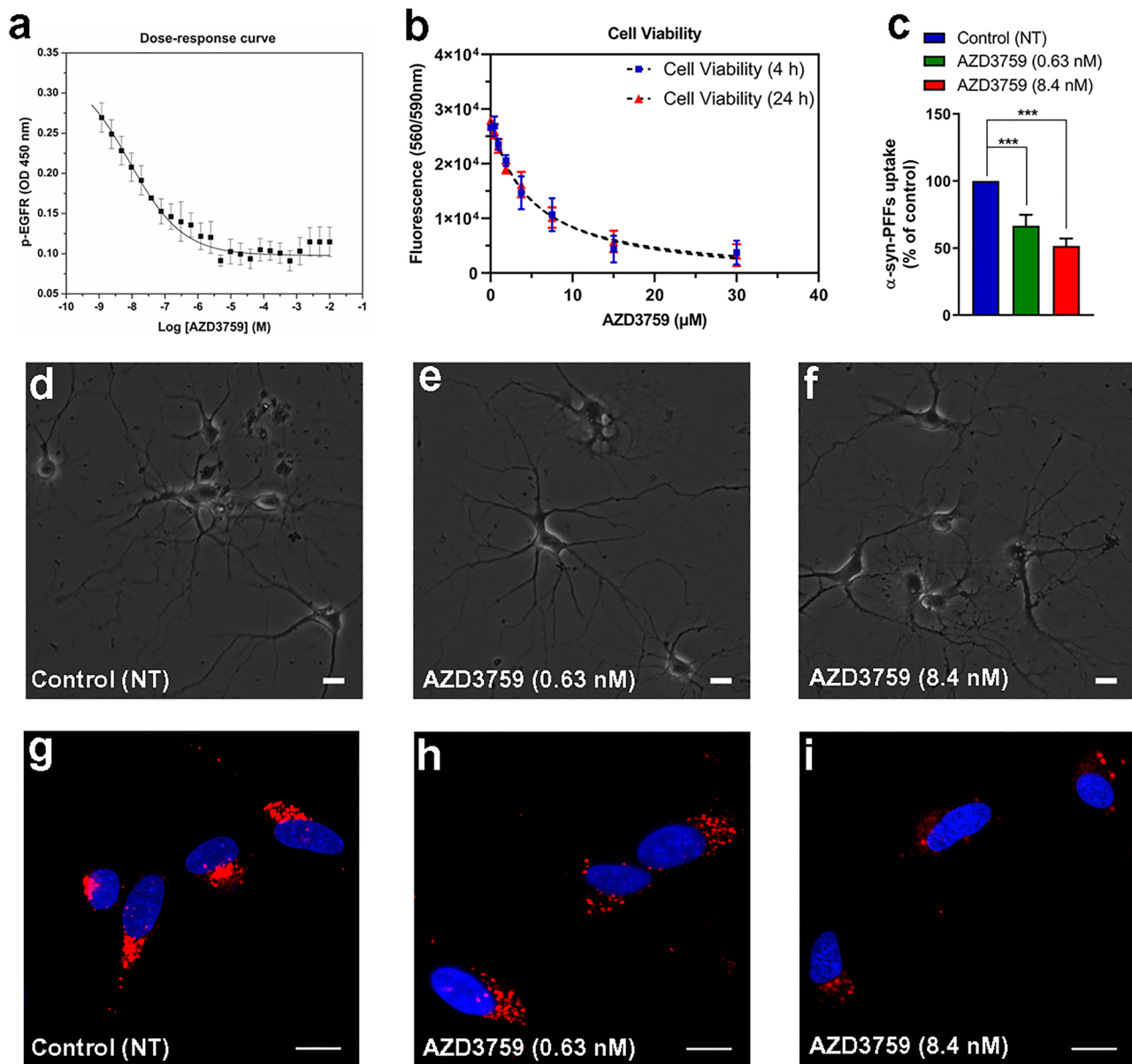


**Fig. 2** AZD3759 activity in mouse cortical neurons. **a** The dose-response curve shows the relationship between AZD3759 concentration and EGFR phosphorylation inhibition in primary mouse cortical neurons. Cells were serum-starved for 2 h and then exposed to AZD3759 at concentrations ranging from 10 to  $1.19209 \times 10^{-6}$  mM. After 4 h of incubation, cells were stimulated with EGF (100 ng/ml) for 20 min. p-EGFR levels of cell lysates were measured using ELISA.  $IC_{20}$  and  $IC_{50}$  (AZD3759 concentrations causing 20% and 50% inhibition of p-EGFR, respectively) values for AZD3759 were measured as 0.63 nM and 8.4 nM, respectively. **b** Viability of mouse primary cortical neurons treated with AZD3759 for 4 h and 24 h. Viability was assessed with CellTiter Blue (Promega).  $LD_{50}$  (AZD3759 concentration causing 50% viability) was measured as 5  $\mu$ M and 4.7  $\mu$ M after 4-h and 24-h incubation times, respectively. **c** Quantification of high-content cellular analysis of  $\alpha$ -syn-PFFs uptake in primary mouse cortical neurons. Neurons grown in culture for 21 days were treated with two concentrations of AZD3759 corresponding to its measured  $IC_{20}$  and  $IC_{50}$  values (0.63 nM

and 8.4 nM, respectively) and incubated for 4 h followed by adding  $\alpha$ -syn-PFFs (100 nM). After 6 h incubation, cells were washed, fixed, and stained with Hoechst 33342 (experiments were repeated three times,  $n=3$ ; three independent biological repeats). **d-f** Images showing mouse cortical neurons cultured for 21 days, treated for 4 h with either AZD3759 (0.63 nM (e) or 8.4 nM (f) or vehicle (d). **g-i** High-content cellular analysis images representing the results shown in c ( $n=3$ ). In each single replicate, 12 different automatically pre-assigned nonoverlapping fields in each well (eight wells for each condition) were imaged. Images from these fields for each condition were selected as representative images. DAPI channel (nucleus) and Cy5 channel (Alexa Fluor 647-labeled  $\alpha$ -syn-PFFs) are represented in blue and red, respectively. The scale bar represents 10  $\mu$ m. Error bars represent mean  $\pm$  SD. One-way ANOVA followed by Tukey's HSD post hoc test was used for statistical comparisons between control (NT) and AZD3759 (0.63 nM and 8.4 nM) treatments ( $F(2,6)=57.58$ , \*\*\* $P \leq 0.001$ )

compared with untreated animals in both PBS- and PFF-injected mice (Fig. 3b–m). Furthermore, we also found that EGFR inhibition decreases the level of  $\alpha$ -syn (Fig. 3d, h, l, m) and pSyn (Fig. S3d, h, m, n). Moreover, no statistically significant difference was detected for the level of pSyn/ $\alpha$ -syn ratio (Fig. S3p, r). A similar reduction in the level of pathogenic A $\beta$  was reported in a mouse model of AD treated with an EGFR inhibitor through induction of autophagy [26]. Thus, we also tested this mode of action using autophagy induction markers (LC3 and p62) [70]. Similar to all other EGFR-TKIs [31, 41, 43–46], AZD3759 also activates autophagy by increasing in the level LC3-II/LC3-I and reduction in the level of p62 (Fig. S3b, c, f, g, i–l, o, q). To confirm this mode of action is due to protein degradation, we measured change in the level of *SCNA* mRNA in this study using quantitative real-time-PCR, and the results showed no significant change in the level of *SNCA* mRNA between mice treated and untreated with AZD3759 (Fig. S3a, e). Next, we performed a proof-of-concept study to test whether AZD3759 can reduce the appearance of pSyn in this same model. The average fibril

length injected to striatum for this study was 30.30 nm. For our proof-of-concept study, neuronal IC<sub>20</sub> and IC<sub>50</sub> concentrations were converted into in vivo doses [71–76] using reported pharmacokinetics values for AZD3759 in animal models to maintain these concentrations in the brain during dosing intervals [53]. The experimental design and dosing regimens for this study are summarized in Fig. 4a and Table 1. Upon completion of dosing, mice were euthanized, and brains were collected for immunohistochemical studies using a specific antibody for pSyn pathology at early stages of seeded pathology upon uptake at the site of injection (striatum) and propagation of pathology to SN. We focused on the site of injection (right dorsal striatum) to measure the inhibitory effect on uptake of recombinant  $\alpha$ -syn-PFFs by neurons in this area and early seeding of endogenous  $\alpha$ -syn aggregation. We also studied pathology development in ipsilateral substantia nigra to measure the inhibitory effect of EGFR inhibition on subsequent uptake and seeding (propagation). First, we found that intrastriatal injection of  $\alpha$ -syn-PFFs resulted in a significant increase in pSyn pathology at the site of injection in the right dorsal

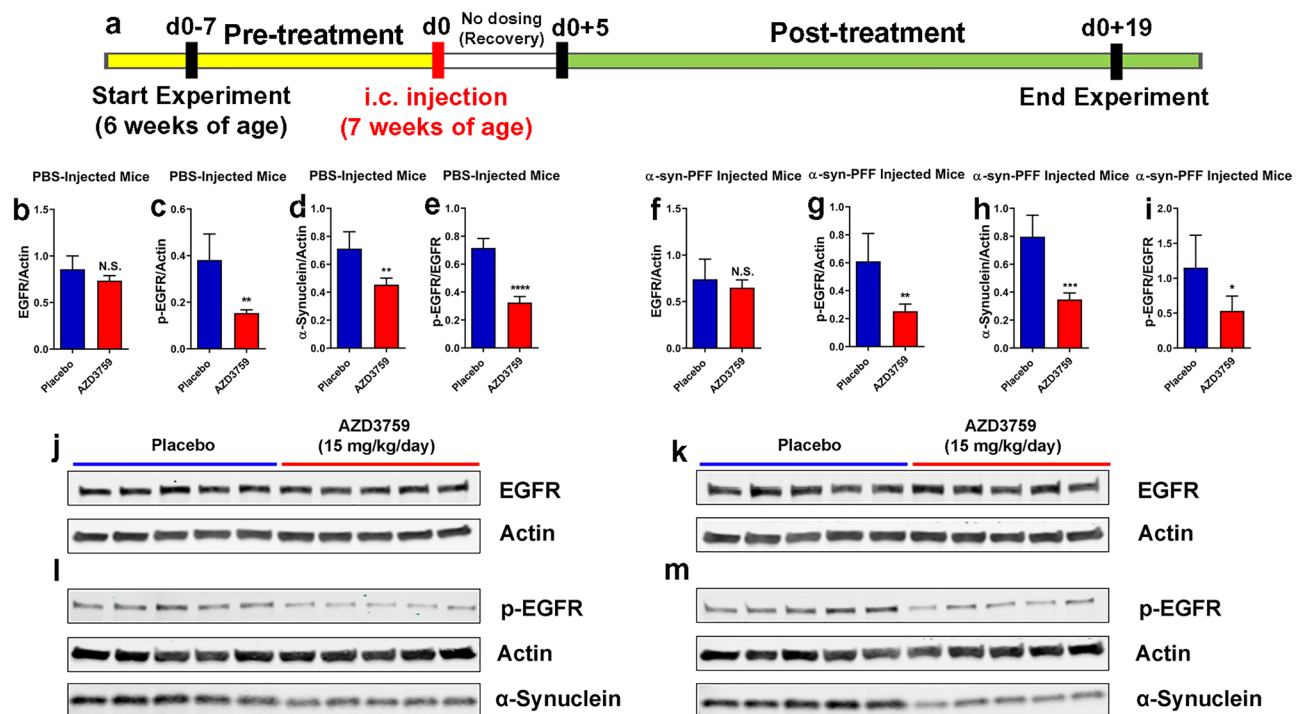
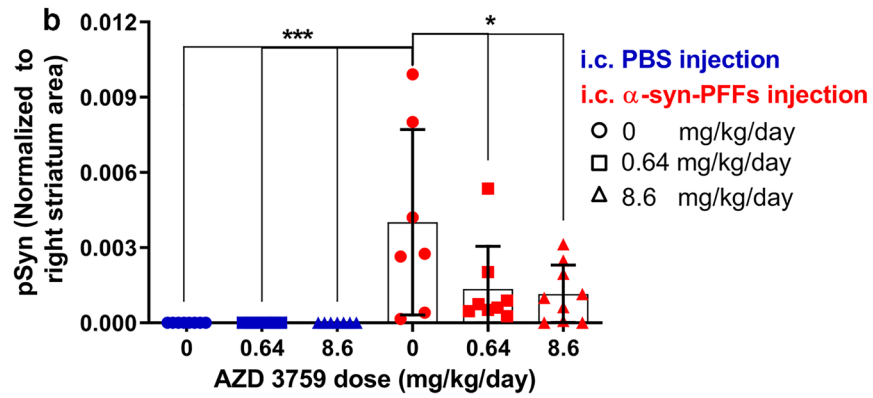
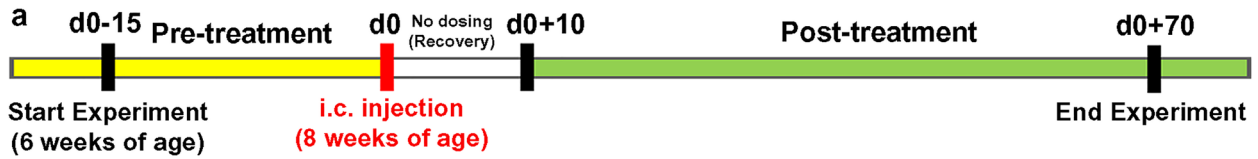


**Fig. 3** Chronic pharmacodynamic study of AZD3759 in mice. **a** Schematic illustration of the experimental design showing the timelines for pre-treatment (7 days), intracerebral (i.c.) inoculation with PBS ( $n=10$ ) or mouse- $\alpha$ -syn-PFFs (average fibril length 50.71 nm) ( $n=10$ ), recovery (5 days), and posttreatment (15 days). Half of the mice ( $n=5$ ) from each group were administrated with placebo (1% methylcellulose) or AZD3759 (15 mg/kg/day). **b–m** Monitoring levels of brain p-EGFR, EGFR, and  $\alpha$ -syn using immunoblot. **b–e, j, l** In PBS-injected mice ( $n=10$ ), administration of AZD3759

(15 mg/kg/day) ( $n=5$ ) resulted in statistical significant reductions in p-EGFR (normalized to actin), activated EGFR (p-EGFR/EGFR) as well as  $\alpha$ -syn. **f–i, k, m** In PFF-injected mice ( $n=10$ ), administration of AZD3759 (15 mg/kg/day) ( $n=5$ ) resulted in statistical significant reductions in p-EGFR (normalized to actin), activated EGFR (p-EGFR/EGFR) as well as  $\alpha$ -syn. Error bars represent mean  $\pm$  SD. The Student's *t* test was used for statistical comparisons between the control (placebo) and the AZD3759 administrated group (\* $P \leq 0.05$ , \*\* $P \leq 0.01$ , \*\*\* $P \leq 0.001$ , and \*\*\*\* $P \leq 0.0001$ )



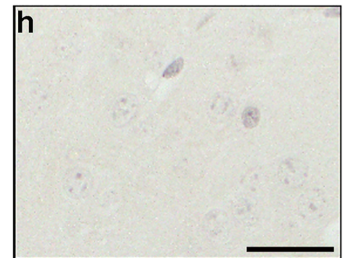
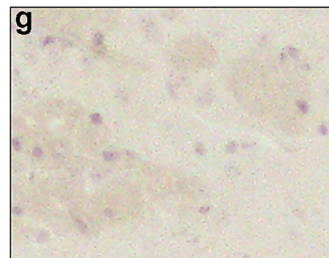
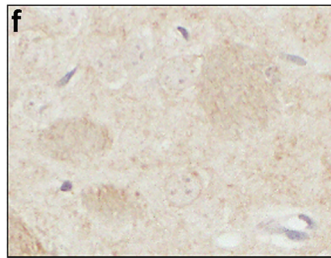
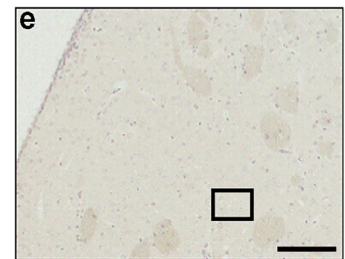
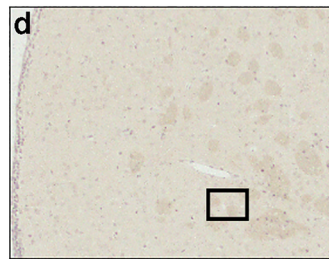
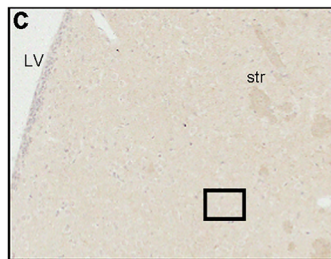
AZD 3759 dose (mg/kg/day):

0 (Placebo)

0.64

8.6

**i.c. PBS injection**



**i.c. -syn-PFFs injection**

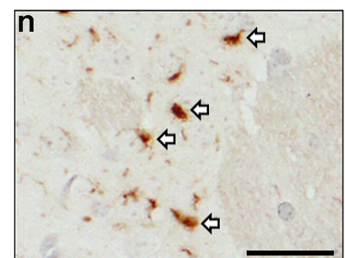
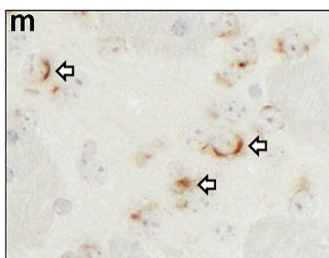
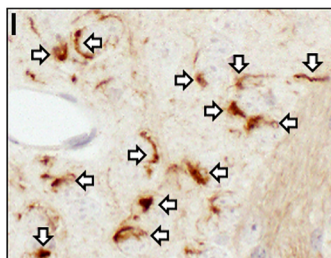
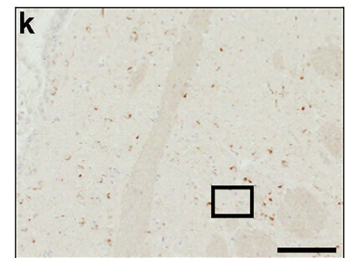
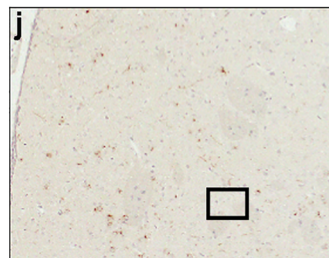
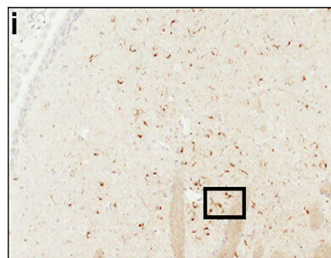


**Fig. 4** AZD3759 decreases  $\alpha$ -syn seeding and propagation in wild-type mice at the level of the right dorsal striatum. **a** Schematic illustration of the experimental design showing the timelines for pretreatment (15 days), intracerebral (i.c.) inoculation with PBS ( $n=22$ ) or mouse- $\alpha$ -syn-PFFs (average fibril length 30.30 nm) ( $n=24$ ), recovery (10 days), and posttreatment (60 days). PBS- and  $\alpha$ -syn-PFFs-injected mice were divided into three subgroups and administrated with placebo (1% methylcellulose), AZD3759 (0.64 mg/kg/day), and AZD3759 (8.6 mg/kg/day). **b** Histogram showing the total phosphorylated pS129  $\alpha$ -synuclein (pSyn) level at dorsal striatum normalized to the corresponding area. Statistical significance in **b** was determined by one-way ANOVA, followed by Tukey's HSD post hoc test ( $F(5,40)=6.126$ ,  $***P=0.0003$ ). **c-n** pSyn immunostaining of coronal sections at the level of the right dorsal striatum (intracerebral injection site) in C57/B6C3F1 mice intracerebrally injected with PBS (**c-e**) or  $\alpha$ -syn-PFFs (**i-k**) and treated with placebo (1% methylcellulose) ( $n=8$  for PBS-injected group and  $n=7$  for the  $\alpha$ -syn-PFFs-injected group), 0.64 mg/kg AZD 3759 ( $n=7$  for PBS-injected group and  $n=8$  for the  $\alpha$ -syn-PFFs-injected group), and 8.6 mg/kg AZD 3759 ( $n=7$  for PBS and  $n=9$  for PFFs). **f-h**, **i-n** Images with high magnification expanded from selected boxes in **c-e** and **i-k** images, respectively, showing pSyn, identified by the brown peroxidase immunoreaction products. No  $\alpha$ -syn pathology was detected in the PBS-injected group. In the  $\alpha$ -syn-PFFs-injection group, the administration of AZD3759 caused significant decreases of pSyn staining at both doses (0.64 and 8.6 mg/kg/day) ( $*P\leq 0.05$ ). Error bars represent mean  $\pm$  SD. Scale bars in **c-e**, **i-k** and **f-h**, **i-n** are 100  $\mu$ m and 20  $\mu$ m, respectively. LV lateral ventricle, str striatum

striatum as compared with PBS-injected wild-type mice ( $***P<0.0001$ ) (Fig. 4b, c, f, i, l). Moreover, the level of pSyn pathology is significantly reduced in PFF-injected mice treated with both doses of AZD3759 compared to the non-treated group ( $*P<0.05$ ) (Fig. 4b, i-n). In the ipsilateral substantia nigra compacta of  $\alpha$ -syn-PFFs injected mice, we could observe a reduction in pSyn pathology (level of pSyn and % pSyn<sup>+</sup> cells) at the low dose (0.64 mg/kg/day) of AZD3759 in comparison to the  $\alpha$ -syn-PFFs-injected group which received Placebo ( $**P<0.01$ ,  $*P<0.05$  respectively) (Fig. 5a, b, i-n). On average, mice injected with  $\alpha$ -syn-PFFs and treated with 0.64 mg/kg/day of AZD3759 had 33% less pSyn<sup>+</sup> cells in the midbrain compared to mice injected with  $\alpha$ -syn-PFFs treated with Placebo (Fig. 5b). Coronal sections were also processed

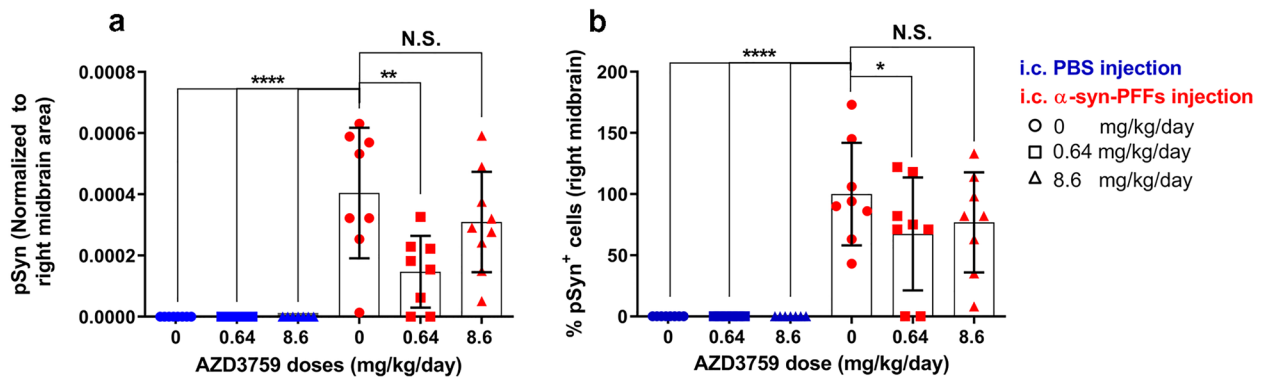
for dual immunofluorescence of pSyn and TH, a marker of dopaminergic neurons (Fig. S2). In  $\alpha$ -syn-PFFs injected mice, while AZD3759 therapy showed a trend towards reducing the level of TH-labeled cells localizing with pSyn, this did not reach statistical significance (Fig. S2a, c-z). Despite in our study (60 dpi) [13, 64], it is unlikely that TH cells undergo degeneration, we also counted the number of TH<sup>+</sup> cells in the SN using the same method that was used to count pSyn<sup>+</sup> cells (Fig. S2b). The results showed no change in the number of TH<sup>+</sup> cells within treated and un-treated groups, suggesting that AZD3759 is not toxic for dopaminergic neurons and the reduction in the level of pSyn pathology is due to a reduction in the level of seeding and propagation of  $\alpha$ -syn, not cell death.

We also performed immunohistochemical staining for EGFR and p-EGFR (Fig. S5). The EGFR-immunoreactive signal was localized in the soma and some primary dendritic branches near the subventricular area of the dorsal striatum and the dorsal striatum (Fig. S5d-f, j-l, p-r, v-x). p-EGFR-immunolabeled signal was observed in the somas of the subventricular area of the dorsal striatum (Fig. S5g-i, m-o, s-u, y-z'). As we discussed in our recently published review, activated EGFR (p-EGFR/EGFR) is an informative pathology associated marker in cancer as well as AD [31]. This marker represents the level of p-EGFR normalized with the total level of EGFR and represents a fraction of the total EGFR, which is activated. The therapeutic effect of EGFR inhibition must target the level of activated EGFR [31]. Thus, we measured the change in the level of activated EGFR in our model (Fig. S5c). Results showed that change in the level of activated EGFR within study groups is statistically significant ( $F(5,42)=3.115$ ,  $*P=0.0176$ ) (Fig. S5c). Furthermore, injection of  $\alpha$ -syn-PFFs increased the level of activated EGFR as compared to PBS-injected mice, and administration of AZD3759 reduced the level of activated EGFR at both doses, but post hoc multiple comparisons showed statistically significant reduction for 8.6 mg/kg/day dose ( $**P<0.01$ ) (Fig. S5c).

**Table 1** Proof-of-concept study groups, including doses and corresponding in vitro concentrations

Mice type	Intrastriatal inoculated	Group	AZD3759 dose (mg/kg/day)	Corresponding in vitro concentrations
Wild type (C57BL6/C3H F1)	PBS	A	Placebo	0
		B	0.64	IC <sub>20</sub> =0.63 nM
		C	8.6	IC <sub>50</sub> =8.4 nM
	Mouse- $\alpha$ -syn-PFFs	D	Placebo	0
		E	0.64	IC <sub>20</sub> =0.63 nM
		F	8.6	IC <sub>50</sub> =8.4 nM

PBS phosphate-buffered saline,  $\alpha$ -syn-PFFs  $\alpha$ -synuclein-pre-formed-fibrils



AZD 3759 dose  
(mg/kg/day):

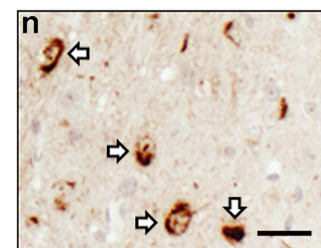
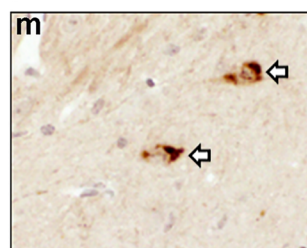
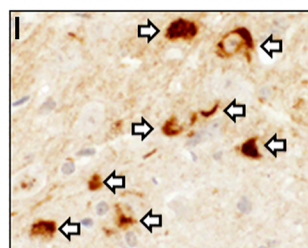
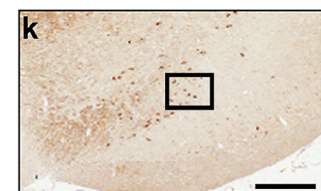
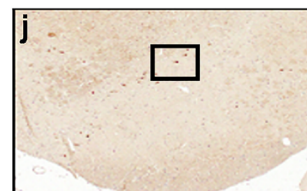
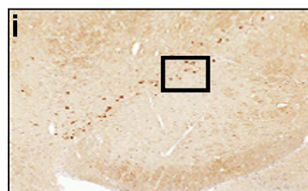
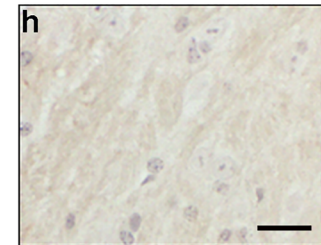
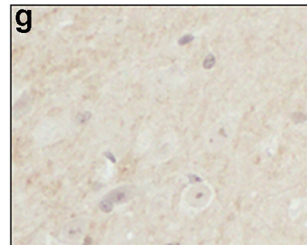
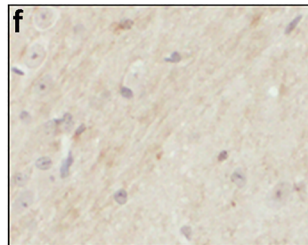
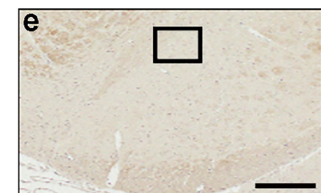
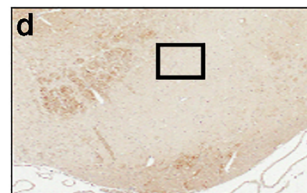
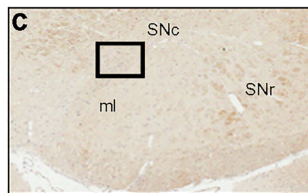
0 (Placebo)

0.64

8.6

i.c. PBS injection

i.c.  $\alpha$ -syn-PFFs injection



## Discussion

Several observations have stimulated our interest in the potential of targeting EGFR using small molecule inhibitors for therapeutic benefit in PD. First, several reports have shown that EGFR is a potential target for developing drugs for treating neurodegenerative diseases [25–27, 29, 36, 37]. For example, EGFR inhibitors are protective in SOD1 [36] and A $\beta$  [26, 27, 37] mice models. The main mechanism

behind the neuroprotective effect of EGFR inhibition in AD is reducing endogenous A $\beta$  through autophagy induction, leading to the reduction of amyloid formation in the brain [26]. Furthermore, it has been shown that fibrils of A $\beta$  [37], huntingtin (polyQ-htt) aggregates [39], and premelanosome protein (PMEL) fibrils [40] bind to cellular EGFR, which propose that EGFR might be involved in the cellular uptake of these oligomers or other similar pathogenic proteins such as  $\alpha$ -syn fibrils. Second, the first selective EGFR

**Fig. 5** AZD3759 decreases  $\alpha$ -syn propagation in wild-type mice at the level of right substantia nigra. **a** Histogram showing the total level of pSyn normalized to ipsilateral midbrain area. Statistical significance in **a** was determined by one-way ANOVA, followed by Tukey's HSD post hoc test ( $F(5,40)=15.48$ , \*\*\*\* $P<0.0001$ ). **b** Histogram showing the % of pSyn<sup>+</sup> cells ([number of pSyn<sup>+</sup> cells/average of pSyn<sup>+</sup> cells of the Placebo-  $\alpha$ -syn-PFFs group)] $\times 100$  at the level of the midbrain. Statistical significance in **b** was determined by one-way ANOVA, followed by Tukey's HSD post hoc test ( $F(5,39)=15.76$ , \*\*\*\* $P<0.0001$ ). **c–n** pSyn immunostaining of coronal sections at the level of the substantia nigra in C57/B6C3F1 mice intracerebrally injected with PBS (**c–e**) or  $\alpha$ -syn-PFFs (average fibril length 30.30 nm) (**i–k**) and treated with 1% methylcellulose (Placebo,  $n=8$ ), 0.64 mg/kg/day of AZD3759 ( $n=6$  for PBS-injected mice and  $n=8$  for  $\alpha$ -syn-PFFs-injected mice) and 8.6 mg/kg/day of AZD3759 ( $n=7$  for PBS-injected group and  $n=9$  for the  $\alpha$ -syn-PFFs-injected group). **f–h**, **l–n** High-magnification images expanded from selected boxes in **c–e** and **i–k** images, respectively, showing pSyn, identified by the brown peroxidase immunoreaction products.  $\alpha$ -Syn pathology was absent in the PBS-injected group. In the  $\alpha$ -syn-PFFs-injected group, significant decreases in the level of pSyn staining (\*\* $P\leq 0.01$ ) as well as % pSyn<sup>+</sup> cells (\* $P\leq 0.05$ ) were observed in the group administered with 0.64 mg/kg/day of AZD3759 in comparison with the Placebo  $\alpha$ -syn-PFFs group. pSyn<sup>+</sup> cells are pointed with a white arrow. Error bars represent mean  $\pm$  SD. Scale bars in **c–e**, **i–k** and **f–h**, **l–n** are 200  $\mu$ m and 20  $\mu$ m, respectively. ml medial lemniscus, SNc substantia nigra compacta, SNr substantia nigra reticulata

inhibitor, AZD3759, which efficiently penetrates the BBB, was recently described [52, 53], and it has been shown that this inhibitor has no apparent toxicity even after long-term dosing over months [50–55]. In this regard, it is notable that AZD3759 has successfully passed phase I clinical trial and even recently entered phase II clinical trials [50, 51, 54, 55].

EGFR is one of the main targets in cancer therapy due to mutations or amplification of the EGFR gene in cancerous cells, which cause uncontrolled cell proliferation and tumor growth. The goal of EGFR-TKI therapy in cancer patients is to reduce or stop the growth and number of tumor cells. Thus, several known and approved EGFR inhibitors are available in the clinic for cancer therapy. Most of these inhibitors target mutant constitutively active forms of EGFR with favorable IC<sub>50</sub> values (nM range) to reduce p-EGFR levels. These inhibitors at doses corresponding to IC<sub>50</sub> values are toxic to cells to stop the proliferation of cancer cells (therapeutic effect) as well as non-cancer cells (side effect) [31]. There is a correlation between activity (IC<sub>50</sub>) and cytotoxicity (LD<sub>50</sub>) of these inhibitors, which capable them of controlling cellular proliferation, to reduce the size of tumors, and prevent downstream outcomes such as spread and metastasis of tumors to other organs [31]. These effects are not desirable in neurodegenerative diseases, but there may be a rationale for targeting the wild-type EGFR. Indeed, it has been shown that in both PD and AD postmortem brain samples from aged patients and animal models, the level of total EGFR is reduced, whereas the level of activated EGFR (p-EGFR/EGFR) is increased [27, 37, 77]. It has been shown that knocking down EGFR or

treatment with an EGFR inhibitor (compound 65) prevents neuronal degeneration due to EGFR activation by ROS in neurons [78, 79].

Besides neuronal degeneration [78, 79], other outcomes of EGFR activation are increase in the level of EGFR-mediated endocytosis of fibrils [37] and inhibition of autophagy [31, 44, 46], which potentially can cause more fibrils uptake and downstream seeding of endogenous  $\alpha$ -syn monomers. Thus, inhibition of EGFR kinase activity is a potential neuroprotective strategy to reduce seeding, propagation, and neurodegeneration through both reduction of fibrils uptake and an increase in autophagy. Therefore, this motivated us to test the neuroprotective potential of EGFR-TKI therapy in a cell culture and a mouse model of  $\alpha$ -syn propagation. Our preliminary cell culture studies showed that reduction in the level of EGFR, as well as treatment of cells with high-affinity EGFR ligands (HB-EGF and EGF), reduce the level of  $\alpha$ -syn-PFFs uptake in cells (Fig. 1). Furthermore, treatment of cells with  $\alpha$ -syn-PFFs activates EGFR over time (Fig. S4). Based on these results and considering the potential effect of EGFR inhibition in targeting the propagation of pathogenic proteins, we tested for the first time the neuroprotective effect of AZD3759, a BBB-penetrating EGFR inhibitor in a mice model of  $\alpha$ -syn propagation. This model provided the possibility to evaluate the inhibitory effect of AZD3759 on both uptake of  $\alpha$ -syn-PFFs as well as the reduction in the level of endogenous  $\alpha$ -syn, which has the potential to decrease subsequent seeding and propagation of  $\alpha$ -syn pathology. Comparing our study with previous reports on treating mice models of AD and ALS with EGFR inhibitor [26, 36, 37], we used a well-characterized BBB-penetrating EGFR inhibitor in this study [52, 53]. Moreover, we have selected concentrations corresponding to neuronal IC<sub>20</sub> and IC<sub>50</sub>, which were non-toxic in neurons in short-term (4 h) and long-term (24 h) incubation times (Fig. 2). At these concentrations, AZD3759 reduces the level of neuronal  $\alpha$ -syn-PFFs uptake (Fig. 2). Furthermore, AZD3759 reduces the levels of p-EGFR, activated EGFR (p-EGFR/EGFR), and endogenous  $\alpha$ -syn (Fig. 3) as well as pSyn (Fig. S3). Moreover, like other EGFR-TKIs [41–45, 47–49], AZD3759 activates autophagy (Fig. S3). Reduction in the level of endogenous  $\alpha$ -syn was not due to a reduction of SNCA mRNA expression (Fig. S3), which suggest that autophagy induction might involve in the degradation of  $\alpha$ -syn proteins. We also observed a significant reduction of pSyn pathology in the striatum of mice treated with AZD3759 at both doses corresponding to neuronal IC<sub>20</sub> and IC<sub>50</sub> (Fig. 4) but only saw a reduction in the ipsilateral substantia nigra at the lower dose (Fig. 5). While having no good explanation for the lack of effect of the higher dose, it is possible that in non-cancer cases, the

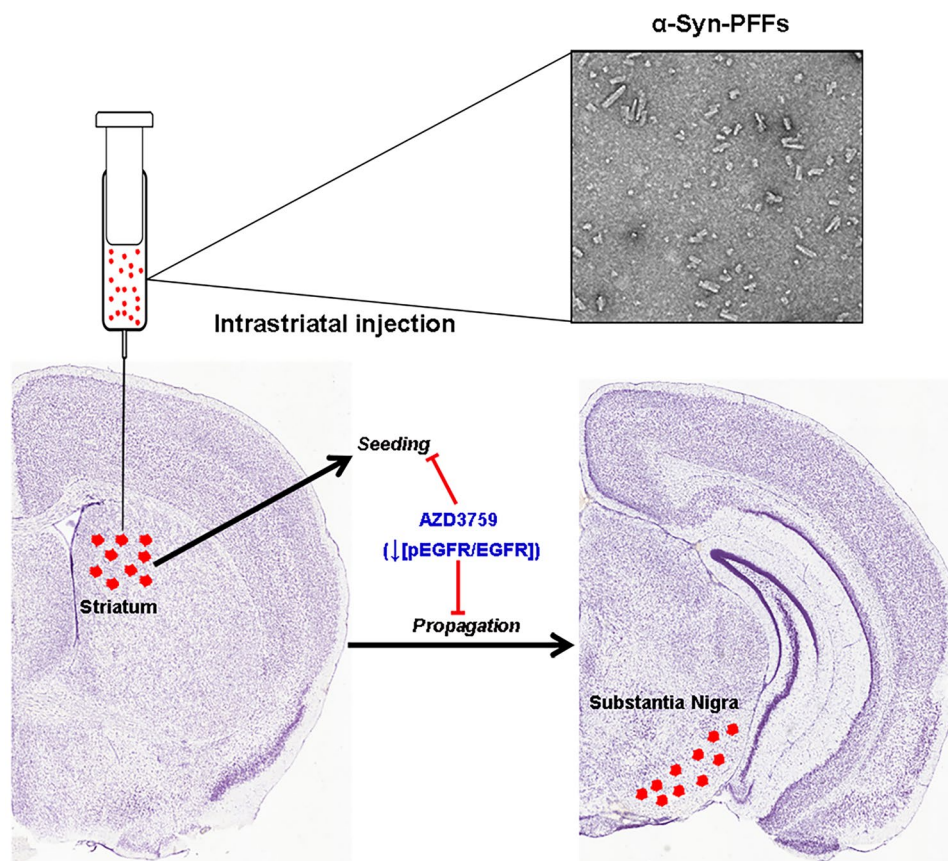
levels and activity of EGFR are lower than cancer cells [31]. In this context, lower concentrations of EGFR-TKI might be sufficient to inhibit EGFR tyrosine kinase activity to a level that can ameliorate  $\alpha$ -syn induced pathology in SN. Another explanation might be the induction of autophagy, which causes resistance in cancer therapy [41, 43–46] but is neuroprotective in neurodegenerative diseases [26, 31] because it reduces the level of endogenous pathogenic and aggregation forming proteins such as amyloid- $\beta$  [26, 31]. The level of resistance or induction of autophagy depends on the administrative dose. Lower doses induce more autophagy induction and resistance compared to higher doses; [80–83] that is why in cancer therapy, high doses of EGFR inhibitors are co-administrated with autophagy inhibitors to avoid resistance and induction of autophagy [42, 47–49]. We have shown that AZD3759 activates autophagy in the brain of mice (Fig. S3). In the case of AZD3759 in our study, the reason that why the lower dose is more effective in reducing pSyn pathology might be because it induces more autophagy efflux than the higher dose. This might lead to more degradation of endogenous  $\alpha$ -syn, which caused less seeding.

Regarding the mechanisms of action of AZD3759, our results suggest that beneficial effect of AZD3759

in this PD mice model is a combination of reduction in  $\alpha$ -syn-PFFs uptake (Fig. 2) and decrease in endogenous  $\alpha$ -syn (Fig. 3) through induction of autophagy (Fig. S3) not reduction of *SCNA* mRNA expression (Fig. S3). The combination of the decrease in both  $\alpha$ -syn-PFFs uptake and endogenous  $\alpha$ -syn leads to a single mode-of-action which is reduction in the propagation-seeding process (Fig. 6).

In all previous EGFR-TKI studies in neurodegenerative diseases, classical EGFR inhibitors with low or unknown levels of BBB penetration were used to evaluate the beneficial effect of EGFR inhibition in neurodegenerative diseases [31]. Therefore, the PK/PD of drugs in the brain was insufficient to conclude their efficacy [31, 36, 37]. In this work, we showed for the first time that EGFR inhibition using a well-characterized BBB-EGFR-TKI leads to a decrease in pSyn pathology in a well-established mouse model of  $\alpha$ -syn propagation. Accordingly, this work represents a potential advance in developing a therapeutic disease-modifying intervention for PD, possibly by repositioning AZD3759. It will be important to confirm these findings in other mice models of PD as well as transgenic mice expressing human EGFR and/or  $\alpha$ -syn considering AZD3759 administration for longer term.

**Fig. 6** AZD3759 mode-of-action: inhibition of EGFR activation by the administration of a BBB-inhibitor (AZD3759) ameliorates  $\alpha$ -syn pathology (pSyn) in a PD mouse model generated by injection of  $\alpha$ -syn-PFFs into the striatum. The beneficial effect of AZD3759 therapy involves the reduction in the seeding at the site of injection as well as propagation to substantia nigra. Brain sections are adopted from Allen Institute (© 2011 Allen Institute for Brain Science. Allen Mouse Brain Atlas. Available from <http://atlas.brain-map.org/>)





**Abbreviations** PFF: Pre-formed-fibril; PD: Parkinson disease; AD: Alzheimer's disease; EGFR: Epidermal growth factor receptor;  $\alpha$ -syn:  $\alpha$ -Synuclein; A $\beta$ PP: Amyloid- $\beta$  protein precursor; A $\beta$ : Amyloid- $\beta$ ;  $\alpha$ -syn-PFFs:  $\alpha$ -Syn-pre-formed-fibrils; HSPG: Heparan sulfate proteoglycan; EM: Electron microscopy; AFM: Atomic force microscopy; PFA: Paraformaldehyde; pSyn: phosphorylated  $\alpha$ -synuclein

**Supplementary Information** The online version contains supplementary material available at <https://doi.org/10.1007/s13311-021-01017-6>.

**Acknowledgements** We thank the Centre for High-Throughput Chemical Biology (HTCB) at the Simon Fraser University for access to research facilities. We thank Dr. David Vocadlo, Dr. Sandeep Bhosale, and Dr. Sachin Kandalkar (Department of Chemistry, Simon Fraser University, Canada) for synthesis and providing AZD3759. This work was supported by the W. Garfield Weston Foundation (Weston Brain Institute) (RR171033) to OT and EAF. EAF is supported by a Canada Research Chair (Tier 1) in Parkinson's Disease and the Canadian Consortium on Neurodegeneration in Aging (CCNA). TMD is supported through funding from the Canada First Research Excellence Fund, awarded to McGill University for the Healthy Brains for Healthy Lives initiative. We thank Dr. Rina Shlaifer, Emmanuelle Nguyen-Renou and Arya Akkus for their help and support with this work. We thank Jefferey Yue for help in cell culture studies. We thank Mateusz Michalik for helping in quantitative reverse-transcriptase PCR.

**Required Author Forms** [Disclosure forms](#) provided by the authors are available with the online version of this article.

**Author Contributions** OT and EAF designed the experiments. OT and ECP performed the experiments, prepared the graphical items, and drafted the manuscript. OT, ECP, and EAF revised and edited the manuscript. VS, RAT, EC, and TMD helped develop the macro for all the IHC quantification, ECP and FL worked to optimize the macro for IF quantification. WL generated the  $\alpha$ -synuclein fibril batches for mouse experiments. ECP characterized the  $\alpha$ -synuclein fibril batches for mouse experiments. TMD and ECP provided input on the macro and image quantification. TMD oversaw the generation and characterization of fibrils for the mouse experiments.

## Declarations

**Conflict of Interest** The authors declare that they have no conflicts of interest.

## References

- Gill C, Phelan JP, Hatzipetros T, et al. SOD1-positive aggregate accumulation in the CNS predicts slower disease progression and increased longevity in a mutant SOD1 mouse model of ALS. *Sci Rep* 2019;9:6724.
- Spires-Jones TL, Attems J, Thal DR. Interactions of pathological proteins in neurodegenerative diseases. *Acta Neuropathol* 2017;134:187-205.
- Irvine GB, El-Agnaf OM, Shankar GM, Walsh DM. Protein aggregation in the brain: the molecular basis for Alzheimer's and Parkinson's diseases. *Molecular medicine (Cambridge, Mass)* 2008;14:451-464.
- Vaquer-Alicea J, Diamond MI. Propagation of Protein Aggregation in Neurodegenerative Diseases. *Annu Rev Biochem* 2019;88:785-810.
- Luk KC, Covell DJ, Kehm VM, et al. Molecular and Biological Compatibility with Host Alpha-Synuclein Influences Fibril Pathogenicity. *Cell Rep* 2016;16:3373-3387.
- Goedert M. Alzheimer's, Parkinson's diseases: The prion concept in relation to assembled A $\beta$ , tau, and  $\alpha$ -synuclein. *Science* 2015;349.
- Volpicelli-Daley LA, Luk KC, Lee VMY. Addition of exogenous  $\alpha$ -synuclein preformed fibrils to primary neuronal cultures to seed recruitment of endogenous  $\alpha$ -synuclein to Lewy body and Lewy neurite-like aggregates. *Nat Protocols* 2014;9:2135-2146.
- Guo JL, Lee VMY. Cell-to-cell transmission of pathogenic proteins in neurodegenerative diseases. *Nat Med* 2014;20:130-138.
- Olanow CW, Brundin P. Parkinson's disease and alpha synuclein: is Parkinson's disease a prion-like disorder? *Mov Disord* 2013;28:31-40.
- Masuda-Suzukake M, Nonaka T, Hosokawa M, et al. Prion-like spreading of pathological  $\alpha$ -synuclein in brain. *Brain* 2013;136:1128-1138.
- Guo Jing L, Covell Dustin J, Daniels Joshua P, et al. Distinct  $\alpha$ -synuclein strains differentially promote tau inclusions in neurons. *Cell* 2013;154:103-117.
- Luk KC, Kehm VM, Zhang B, et al. Intracerebral inoculation of pathological  $\alpha$ -synuclein initiates a rapidly progressive neurodegenerative  $\alpha$ -synucleinopathy in mice. *The Journal of Experimental Medicine* 2012;209:975-986.
- Luk KC, Kehm V, Carroll J, et al. Pathological  $\alpha$ -Synuclein Transmission Initiates Parkinson-like Neurodegeneration in Nontransgenic Mice. *Science* 2012;338:949-953.
- Volpicelli-Daley Laura A, Luk Kelvin C, Patel Tapan P, et al. Exogenous  $\alpha$ -synuclein fibrils induce Lewy body pathology leading to synaptic dysfunction and neuron death. *Neuron* 2011;72:57-71.
- Hansen C, Angot E, Bergstr, et al.  $\alpha$ -Synuclein propagates from mouse brain to grafted dopaminergic neurons and seeds aggregation in cultured human cells. *The Journal of Clinical Investigation* 2011;121:715-725.
- Desplats P, Lee H-J, Bae E-J, et al. Inclusion formation and neuronal cell death through neuron-to-neuron transmission of  $\alpha$ -synuclein. *Proceedings of the National Academy of Sciences* 2009;106:13010-13015.
- Vogels T, Leuzy A, Cicognola C, et al. Propagation of Tau Pathology: Integrating Insights From Postmortem and In Vivo Studies. *Biol Psychiatry* 2020;87:808-818.
- Hallinan GI, Vargas-Caballero M, West J, Deinhardt K. Tau Misfolding Efficiently Propagates between Individual Intact Hippocampal Neurons. *The Journal of Neuroscience* 2019;39:9623.
- Eisele YS, Monteiro C, Fearn C, et al. Targeting protein aggregation for the treatment of degenerative diseases. *Nature reviews Drug discovery* 2015;14:759-780.
- Zhang Z, Nie S, Chen L. Targeting prion-like protein spreading in neurodegenerative diseases. *Neural Regeneration Research* 2018;13:1875-1878.
- Aboutit S, Bousset L, Loria F, et al. Tunneling nanotubes spread fibrillar  $\alpha$ -synuclein by intercellular trafficking of lysosomes. *The EMBO Journal* 2016;35:2120-2138.
- Dieriks BV, Park TI, Fourie C, et al. alpha-synuclein transfer through tunneling nanotubes occurs in SH-SY5Y cells and primary brain pericytes from Parkinson's disease patients. *Sci Rep* 2017;7:42984.
- Holmes BB, DeVos SL, Kfoury N, et al. Heparan sulfate proteoglycans mediate internalization and propagation of specific proteopathic seeds. *Proceedings of the National Academy of Sciences* 2013;110:E3138-E3147.
- Mao X, Ou MT, Karuppagounder SS, et al. Pathological  $\alpha$ -synuclein transmission initiated by binding lymphocyte-activation gene 3. *Science* 2016;353.
- Chen X, Wang C, Zhou S, Li X, Wu L. The Impact of EGFR Gene Polymorphisms on the Risk of Alzheimer's Disease in a Chinese Han Population: A Case-Controlled Study. *Med Sci Monit* 2018;24:5035-5040.
- Wang B-J, Her GM, Hu M-K, et al. ErbB2 regulates autophagic flux to modulate the proteostasis of APP-CTFs in Alzheimer's disease. *Proceedings of the National Academy of Sciences* 2017;114:E3129-E3138.

27. Wang L, Liang B, Zhong Y. Reduced EGFR level potentially mediates the A $\beta$ 2-induced neuronal loss in transgenic fruit fly and mouse. *Protein & Cell* 2013;4:647-649.
28. Qu W-s, Tian D-s, Guo Z-b, et al. Inhibition of EGFR/MAPK signaling reduces microglial inflammatory response and the associated secondary damage in rats after spinal cord injury. *J Neuroinflammation* 2012;9:178.
29. Chiang H-C, Wang L, Xie Z, Yau A, Zhong Y. PI3 kinase signaling is involved in A $\beta$ -induced memory loss in *Drosophila*. *Proceedings of the National Academy of Sciences* 2010;107:7060-7065.
30. Jin J, Xue L, Bai X, et al. Association between epidermal growth factor receptor gene polymorphisms and susceptibility to Parkinson's disease. *Neurosci Lett* 2020;736:135273.
31. Tavassoly O, Sato T, Tavassoly I. Inhibition of Brain Epidermal Growth Factor Receptor Activation: A Novel Target in Neurodegenerative Diseases and Brain Injuries. *Mol Pharmacol* 2020;98:13-22.
32. Hu W, Zhang S, Shen Y, Yang Q. Epidermal growth factor receptor is a co-factor for transmissible gastroenteritis virus entry. *Virology* 2018;521:33-43.
33. Zheng K, Kitazato K, Wang Y. Viruses exploit the function of epidermal growth factor receptor. *Rev Med Virol* 2014;24:274-286.
34. Ueki IF, Min-Oo G, Kalinowski A, et al. Respiratory virus-induced EGFR activation suppresses IRF1-dependent interferon lambda and antiviral defense in airway epithelium. *J Exp Med* 2013;210:1929-1936.
35. Diao J, Pantua H, Ngu H, et al. Hepatitis C Virus Induces Epidermal Growth Factor Receptor Activation via CD81 Binding for Viral Internalization and Entry. *J Virol* 2012;86:10935-10949.
36. Le Pichon CE, Dominguez SL, Solano H, et al. EGFR inhibitor erlotinib delays disease progression but does not extend survival in the SOD1 mouse model of ALS. *PLoS One* 2013;8:e62342.
37. Wang L, Chiang H-C, Wu W, et al. Epidermal growth factor receptor is a preferred target for treating Amyloid- $\beta$ -induced memory loss. *Proceedings of the National Academy of Sciences* 2012;109:16743-16748.
38. Iwamoto M, Saso W, Sugiyama R, et al. Epidermal growth factor receptor is a host-entry cofactor triggering hepatitis B virus internalization. *Proceedings of the National Academy of Sciences* 2019;116:8487-8492.
39. Melone MAB, Calarco A, Petillo O, et al. Mutant huntingtin regulates EGF receptor fate in non-neuronal cells lacking wild-type protein. *Biochim Biophys Acta (BBA) - Mol Basis Dis* 2013;1832:105-113.
40. Tomas A, Vaughan SO, Burgoyne T, et al. WASH and Tsg101/ALIX-dependent diversion of stress-internalized EGFR from the canonical endocytic pathway. *Nature Communications* 2015;6:7324.
41. Wu M, Zhang P. EGFR-mediated autophagy in tumorigenesis and therapeutic resistance. *Cancer Lett* 2020;469:207-216.
42. Kwon Y, Kim M, Jung HS, Kim Y, Jeoung D. Targeting Autophagy for Overcoming Resistance to Anti-EGFR Treatments. *Cancers (Basel)* 2019;11.
43. Aveic S, Tonini GP. Resistance to receptor tyrosine kinase inhibitors in solid tumors: can we improve the cancer fighting strategy by blocking autophagy? *Cancer Cell Int* 2016;16:62.
44. Fung C, Chen X, Grandis JR, Duvvuri U. EGFR tyrosine kinase inhibition induces autophagy in cancer cells. *Cancer Biol Ther* 2012;13:1417-1424.
45. Han W, Pan H, Chen Y, et al. EGFR tyrosine kinase inhibitors activate autophagy as a cytoprotective response in human lung cancer cells. *PLoS One* 2011;6:e18691.
46. Wei Y, Zou Z, Becker N, et al. EGFR-mediated Beclin 1 phosphorylation in autophagy suppression, tumor progression, and tumor chemoresistance. *Cell* 2013;154:1269-1284.
47. Wang X, Li W, Zhang N, Zheng X, Jing Z. Opportunities and challenges of co-targeting epidermal growth factor receptor and autophagy signaling in non-small cell lung cancer. *Oncol Lett* 2019;18:499-506.
48. Wang Z, Du T, Dong X, et al. Autophagy inhibition facilitates erlotinib cytotoxicity in lung cancer cells through modulation of endoplasmic reticulum stress. *Int J Oncol* 2016;48:2558-2566.
49. Zou Y, Ling YH, Sironi J, et al. The autophagy inhibitor chloroquine overcomes the innate resistance of wild-type EGFR non-small-cell lung cancer cells to erlotinib. *J Thorac Oncol* 2013;8:693-702.
50. Cho BC, Ahn M-J, Lee J-S, et al. Phase I study (BLOOM) of AZD3759, a BBB penetrable EGFR inhibitor, in EGFRm NSCLC patients with leptomeningeal metastasis (LM) who progressed after other anti-cancer therapy. *J Clin Oncol* 2017;35:2069-2069.
51. Ahn M-J, Kim D-W, Cho BC, et al. Phase I study (BLOOM) of AZD3759, a BBB penetrable EGFR inhibitor, in patients with TKI-naïve, EGFRm NSCLC with CNS metastases. *J Clin Oncol* 2017;35:2006-2006.
52. Yang Z, Guo Q, Wang Y, et al. AZD3759, a BBB-penetrating EGFR inhibitor for the treatment of EGFR mutant NSCLC with CNS metastases. *Sci Transl Med* 2016;8:368ra172-368ra172.
53. Zeng Q, Wang J, Cheng Z, et al. Discovery and Evaluation of Clinical Candidate AZD3759, a Potent, Oral Active, Central Nervous System-Penetrant, Epidermal Growth Factor Receptor Tyrosine Kinase Inhibitor. *J Med Chem* 2015;58:8200-8215.
54. Li X, Wang Y, Wang J, et al. Enhanced efficacy of AZD3759 and radiation on brain metastasis from EGFR mutant non-small cell lung cancer. 2018;143:212-224.
55. Ahn M-J, Kim D-W, Kim TM, et al. Phase I study of AZD3759, a CNS penetrable EGFR inhibitor, for the treatment of non-small-cell lung cancer (NSCLC) with brain metastasis (BM) and leptomeningeal metastasis (LM). *J Clin Oncol* 2016;34:9003-9003.
56. Tavassoly O, Yue J, Vocadlo DJ. Pharmacological inhibition and knockdown of O-GlcNAcase reduces cellular internalization of  $\alpha$ -synuclein preformed fibrils. *The FEBS Journal* 2021;288:452-470.
57. Tavassoly O, Sade D, Bera S, et al. Quinolinic Acid Amyloid-like Fibrillar Assemblies Seed  $\alpha$ -Synuclein Aggregation. *J Mol Biol* 2018;430:3847-3862.
58. Masuda-Suzukake M, Nonaka T, Hosokawa M, et al. Pathological alpha-synuclein propagates through neural networks. *Acta Neuropathol Commun* 2014;2:88.
59. Masuda-Suzukake M, Nonaka T, Hosokawa M, et al. Prion-like spreading of pathological alpha-synuclein in brain. *Brain* 2013;136:1128-1138.
60. Faul F, Erdfelder E, Buchner A, Lang A-G. Statistical power analyses using G\*Power 3.1: Tests for correlation and regression analyses. *Behav Res Methods* 2009;41:1149-1160.
61. Faul F, Erdfelder E, Lang A-G, Buchner A. G\*Power 3: A flexible statistical power analysis program for the social, behavioral, and biomedical sciences. *Behav Res Methods* 2007;39:175-191.
62. Chung HK, Ho HA, Pérez-Acuña D, Lee SJ. Modeling  $\alpha$ -Synuclein Propagation with Preformed Fibril Injections. *J Mov Disord* 2019;12:139-151.
63. Blumenstock S, Rodrigues EF, Peters F, et al. Seeding and transgenic overexpression of alpha-synuclein triggers dendritic spine pathology in the neocortex. *EMBO Mol Med* 2017;9:716-731.
64. Abdelmotilib H, Maltbie T, Delic V, et al.  $\alpha$ -Synuclein fibril-induced inclusion spread in rats and mice correlates with dopaminergic Neurodegeneration. *Neurobiol Dis* 2017;105:84-98.
65. Schindelin J, Arganda-Carreras I, Frise E, et al. Fiji: an open-source platform for biological-image analysis. *Nat Methods* 2012;9:676-682.
66. Lee BR, Kamitani T. Improved immunodetection of endogenous  $\alpha$ -synuclein. *PLoS One* 2011;6:e23939.
67. Tavassoly O, Nokhrin S, Dmitriev OY, Lee JS. Cu(II) and dopamine bind to  $\alpha$ -synuclein and cause large conformational changes. *The FEBS Journal* 2014;281:2738-2753.
68. Tavassoly O, Lee JS. Methamphetamine binds to  $\alpha$ -synuclein and causes a conformational change which can be detected by nanopore analysis. *FEBS Lett* 2012;586:3222-3228.

69. Tavassoly O, Kakish J, Nokhrin S, Dmitriev O, Lee JS. The use of nanopore analysis for discovering drugs which bind to  $\alpha$ -synuclein for treatment of Parkinson's disease. *Eur J Med Chem* 2014;88:42-54.
70. Klionsky DJ, Abdelmohsen K, Abe A, et al. Guidelines for the use and interpretation of assays for monitoring autophagy (3rd edition). *Autophagy* 2016;12:1-222.
71. Tirona RG, Kim RB. Chapter 20 - Introduction to Clinical Pharmacology. In: Robertson D, Williams GH, editors. *Clinical and Translational Science (Second Edition)*: Academic Press; 2017. p. 365-388.
72. Muir Iii WW. Chapter 15 - Factors Influencing Analgesic Drug Selection, Dose, and Routes of Drug Administration. *Handbook of Veterinary Pain Management (Third Edition)*. St. Louis: Mosby; 2015. p. 302-334.
73. Holford NHG. Chapter 3 - Pharmacokinetics & Pharmacodynamics: Rational Dosing & the Time Course of Drug Action In: Katzung BG, Masters SB, Trevor AJ, editors. *Basic & clinical pharmacology (12th Edition)*. New York: Lange Medical Books/McGraw Hill; 2012. p. 37-51.
74. Tirona RG, Kim RB. Chapter 22 - Introduction to Clinical Pharmacology. In: Robertson D, Williams GH, editors. *Clin Transl Sci*. San Diego: Academic Press; 2009. p. 321-338.
75. Muir Iii WW, Sams RA. Chapter 7 - Pharmacologic Principles and Pain: Pharmacokinetics and Pharmacodynamics. *Handbook of Veterinary Pain Management (Second Edition)*. Saint Louis: Mosby; 2009. p. 113-140.
76. Buxton LLO. Chapter 1 - Pharmacokinetics: the dynamics of drug absorption, distribution, metabolism, and elimination In: Brunton LL, Lazo JS, Parker KL, editors. *Goodman & Gilman's the pharmacological basis of therapeutics (11th Edition)*. New York: McGraw-Hill; 2006. p. 1-39.
77. Iwakura Y, Piao Y-s, Mizuno M, et al. Influences of dopaminergic lesion on epidermal growth factor-ErbB signals in Parkinson's disease and its model: neurotrophic implication in nigrostriatal neurons. *J Neurochem* 2005;93:974-983.
78. Wakatsuki S, Araki T. NADPH oxidases promote apoptosis by activating ZNRF1 ubiquitin ligase in neurons treated with an exogenously applied oxidant. *Commun Integr Biol* 2016;9:e1143575.
79. Wakatsuki S, Furuno A, Ohshima M, Araki T. Oxidative stress-dependent phosphorylation activates ZNRF1 to induce neuronal/axonal degeneration. *The Journal of Cell Biology* 2015;211:881-896.
80. Hayakawa H, Ichihara E, Ohashi K, et al. Lower gefitinib dose led to earlier resistance acquisition before emergence of T790M mutation in epidermal growth factor receptor-mutated lung cancer model. *Cancer Sci* 2013;104:1440-1446.
81. Chmielecki J, Foo J, Oxnard GR, et al. Optimization of dosing for EGFR-mutant non-small cell lung cancer with evolutionary cancer modeling. *Sci Transl Med* 2011;3:90ra59.
82. Godin-Heymann N, Ulkus L, Brannigan BW, et al. The T790M "gatekeeper" mutation in EGFR mediates resistance to low concentrations of an irreversible EGFR inhibitor. *Mol Cancer Ther* 2008;7:874-879.
83. Yang L, Ying S, Hu S, et al. EGFR TKIs impair lysosome-dependent degradation of SQSTM1 to compromise the effectiveness in lung cancer. *Signal Transduction and Targeted Therapy* 2019;4:25.

**Publisher's Note** Springer Nature remains neutral with regard to jurisdictional claims in published maps and institutional affiliations.